Ocean Engineering 266 (2022) 112787

Contents lists available at ScienceDirect

Ocean Engineering

journal homepage: www.elsevier.com/locate/oceaneng

An improved BEMT model based on agent actuating disk with application to ship self-propulsion simulation

Mingzhe Wang, Decheng Wan, Jianhua Wang *

Computational Marine Hydrodynamics Lab (CMHL), School of Naval Architecture, Ocean and Civil Engineering, Shanghai Jiao Tong University, Shanghai, 200240, China

A R T I C L E I N F O

Keywords:
Agent actuating disk
Blade element momentum theory
Body-force model
Propeller open-water test
Ship self-propulsion simulation

A B S T R A C T

Propeller body-force model is a low-cost tool for numerical simulation of the ship self-propulsion test compared with discretized propeller model. As one of the most traditional theories of propeller model, Blade Element Momentum Theory (BEMT) has been proved to have considerable application potential with stability and accuracy. However, it's still hard for BEMT to keep accuracy in a relatively large range of working conditions due to unproved prior assumptions, which limits the application of BEMT in complex inflow conditions like ship self-propulsion. In the application of BEMT, the calculation method of Angle of Attack (AOA) has a great influence on the accuracy. In this paper, an "Agent Actuating Disk (AAD)" method is proposed to determine the AOA. AAD-BEMT method uses AAD to obtain the relationship between local velocity and inflow velocity so that the AOA can be defined by geometric Angle of Attack. This consideration avoids the inaccuracy of determining AOA by local velocity from discretized propeller flow field. The KP505 propeller open-water test is chosen to verify the accuracy of the proposed AAD-BEMT method. Then the numerical simulation of a KRISO Container Ship (KCS) self-propulsion test (Fr = 0.26) is carried out to investigate the performance of the AAD-BEMT body-force model as well as other different propeller models when dealing with non-uniform ship's wake. The open-water curve, propeller load distribution, and self-propulsion factor are presented and compared with the available experimental data. The results show that the predicted load distribution is accurate. In addition, not only the thrust and torque of the AAD-BEMT model can have a stable accuracy in a wide operating condition, but also the wake agrees well with the experimental result, which means that the proposed AAD-BEMT model can economically and accurately simulate the momentum transport of propeller under complex hull-propeller interaction condition.

1. Introduction

Computational Fluid Dynamics (CFD) has been widely used in the research field of ship hydrodynamics. By solving governing equations in the fluid domains with complex geometry, CFD methods have the advantage in obtaining the hydrodynamic information of marine structures over using expensive experimental equipment. However, it still needs a large amount of computational resources for some complex hydrodynamic problems, such as hull-propeller interactions. The complex geometrical structure of a propeller requires almost the same number of mesh elements as that of a ship hull (Shen et al., 2015), and the large mesh distortion limits the time-step, which is very unfavorable for the simulation of a long period of a ship self-propulsion test.

It is a general idea to reduce the simulation cost of complex structures interacting with each other by setting the source term force field instead of the discretization of complex geometries, such as the immersed-boundary method (Posa and Broglia, 2019) or centripetal force model (Yu and Wang, 2020; Liu et al., 2021). The body-force method introduces the force source term into the flow field numerically and does not need to generate the propeller mesh. This is a popular research idea to deal with the interaction between complex structures and ship hulls recently. This method effectively avoids the problem of geometrical discontinuity caused by propeller mesh rotation.

Body-force models can be divided into the descriptive body-force models (Hough and Ordway, 1965) and the iterative body-force models (Phillips et al., 2009; Benini, 2004). The force distribution of the descriptive body-force models are determined before the simulation, and the influence of inflow on the propeller performance is not

* Corresponding author.
E-mail address: jianhuawang@sjtu.edu.cn (J. Wang).

https://doi.org/10.1016/j.oceaneng.2022.112787
Received 11 July 2022; Received in revised form 14 September 2022; Accepted 1 October 2022
Available online 31 October 2022

considered. By contrast, the iterative body-force models will update the force distribution according to the influence of the flow field on the propeller load.

The earliest descriptive body-force model is the HO model (Hough and Ordway, 1965), and it has been widely used in the ship self-propulsion test simulation (Zhang, 2010; Kim et al., 2021; Yao et al., 2021). Based on the HO propeller model and structured grid, Fu et al. (2015) carried out the self-propulsion simulation of the KCS ship model and deduced the method of calculating propeller inflow velocity by local velocity. In recent years, as the CFD simulation method of propeller open-water test based on viscous solver is gradually matured, some scholars begin to take blade element load obtained from the CFD result as the direct input of the descriptive body-force model. Villa et al. (2018, 2020) studied the propeller-rudder interaction based on the descriptive body-force model. In their study, the distribution of body-force was obtained from the radial load distribution from the open-water test by discretized propeller model. The results showed that the simulation are good under the condition of small rudder angles, but the accuracy of the descriptive body-force model was decreased when the rudder angle increases to affect the income flow.

Iterative body-force models, such as the boundary element propeller models (Guo et al., 2020), the lift line propeller models (Simonsen and Stern, 2005), and the blade element momentum theory models (Benini, 2004) can deal with non-uniform inflow problems. The accuracy and complexity of the traditional blade element momentum theory model are in the middle position among different body-force models (Phillips et al., 2009). Traditional BEMT has been widely used in marine engineering like propeller design, self-propulsion with hull-propeller interaction, and ship maneuverability with hull-propeller-rudder interaction. Phillips et al. (2010) conducted rudder-propeller interaction simulation based on the Uniform Thrust (UT) distribution model, HO model, and BEMT model. The results showed that the BEMT model has the best agreement among the three models. It proved that when the blade shape is considered, the rotating action of the blade can be ignored, which meant by placements the source term representing the blade element in the propeller plane, steady-state simulation can be used to replace real propeller instantaneous simulation. The same conclusion was reached by Ren et al. (2020), which provided the development of wake around the rudder. However, these studies did not give the results at different advance ratios. Broglia et al. (2013) used HO model, BEMT model, and modified HO model to simulate ship maneuverability test, and found that although BEMT is better than the traditional HO model, it still has an error of around 10% on trajectories and kinematic results, and modified HO model with extra side force works better. Phillips et al. (2009) studied the influence of rudder angle and drift angle on the hull-propeller-rudder system based on BEMT theory, the results showed that the data trend of hull force and rudder force was in good agreement but the propeller thrust was overestimated. The above research shows that BEMT theory can reflect the performance of the discretized propeller to a certain extent, but its accuracy has a large space to improve in complex working conditions.

There are two points of the numerical error in BEMT. One is the inaccuracy of the force coefficient of the blade element, and the other is the inaccuracy of the Angle of Attack (AOA) of the blade element. For the first point, the traditional blade element force coefficient is expressed by empirical formulas derived from 2D-airfoil experiments. Ortolani et al. (2018) modified the empirical formula of airfoil parameters based on the linear cavitation theory and calculated the propeller load in the off-design after-ship condition based on the BEMT body-force model in oblique flows. They suggested that the trend and magnitude of load obtained by BEMT method were the same as those obtained by the experiment, but the absolute error was still very high. Benini (2004) used BEMT to calculate the open-water data of heavy-load propellers, and the blade element force coefficient was obtained by using the airfoil analysis program *Xfoil* based on potential flow theory to calculate the lifting/drag coefficient of the discretized propeller blade section. The results showed that the error of the BEMT increased greatly when the advance ratio velocity was relatively high or low due to the large radial flow on the propeller blade. Li et al. (2019) proposed a fitting formula of propeller blade element force coefficient based on an empirical formula, and obtained the fitting coefficient by regressing blade element performance parameters of discretized propeller model. This method has been used in the simulation of the ship self-propulsion test in the subsequent literature such as Feng et al. (2020,b) and Yu et al. (2021), but there were still large errors at higher and lower advance speeds (Yu et al., 2021). Further, because the three-dimensional viscosity solver does not satisfy the ideal fluid theory and the blade element theory of BEMT, the traditional BEMT may deviate from the actual situation in solving the effective inflow velocity and induct factor iteratively.

For the second point, there are two ways to define the AOA: effective AOA defined by local velocity and geometric AOA defined by inflow velocity. On the one hand, the traditional BEMT is based on the geometric AOA, and the model calculates the inflow velocity according to iteratively solving the inducing factor based on the ideal fluid hypothesis. In the viscosity solver, the body-force model will produce an error because the ideal fluid hypothesis is not satisfied. On the other hand, it is difficult to define the blade AOA based on the effective AOA in the application of body-force model. Although research progresses have been made on extracting the AOA of an airfoil from real turbine structures by using the 3D CFD flow fields (Shen et al., 2009; Vimalakanthan et al., 2018; Melani et al., 2020), all of them focus on wind turbines. No relevant research has been found on marine propellers with large area ratios yet. Meanwhile, due to the difference between the local velocity of the flow field induced by the airfoil and the source term, the local velocity of a body-force model can hardly represent that of an airfoil. Yamazaki (1977) proposed to directly use the local velocity of the flow field at the position of the blade element to calculate the hydrodynamic force, and gave the theoretical formula of blade element lifting/drag coefficient. Tokgoz et al. (2014) applied this method to a viscosity solver and studied the open-water performance accuracy of the BEMT model and an oblique flow state based on the KP505 propeller model. Because there is no need to solve the induction factor iteratively, this method saves the calculation time and the open-water curve simulation is relatively accurate at a higher advance rate, but the thrust calculation results become significantly larger at a lower advance than that of a discretized propeller model. This model has also been applied to the hull-propeller interaction simulation (Win et al., 2013, Naing Win et al., 2016; Windén et al., 2015). Li et al. (2019), Feng et al. (2020, b) and Yu et al. (2021) used the same scheme to deal with local velocity. When extracting the performance of the blade element under discretized propeller load, Yu et al. (2021) used the average velocity of the annular region swept by the blade element in the propeller plane as the local velocity of the blade element. However, the representativeness of this method has not been proved yet, which may be the reason why the error is sensitive to the advance ratio.

To sum up, direct use of local velocity of the flow field is a way to replace iterative solution based on momentum theory, but this will make it difficult to define the lifting/drag coefficient of blade element. At least the current method cannot satisfy the accuracy in a wide range of operating conditions. Due to the non-uniform distribution of advance velocity at the propeller plane in the ship self-propulsion test, the body-force model with accuracy sensitive to advance velocity cannot fully reflect the working state of a propeller.

In this paper, an improved BEMT body-force model based on Agent Actuating Disk (AAD) is proposed. The force coefficient of the blade element is calculated based on the pressure and friction integration of the blade surface in open-water simulation. The definition of blade AOA is based on the geometric AOA, and the relationship between local velocity and incoming velocity is obtained by AAD. To ensure the fitting accuracy, the linear interpolation method is used to calculate the force coefficient and inflow velocity. In this paper, the KP505 open-water simulation is carried out, and the convergence of data is discussed.

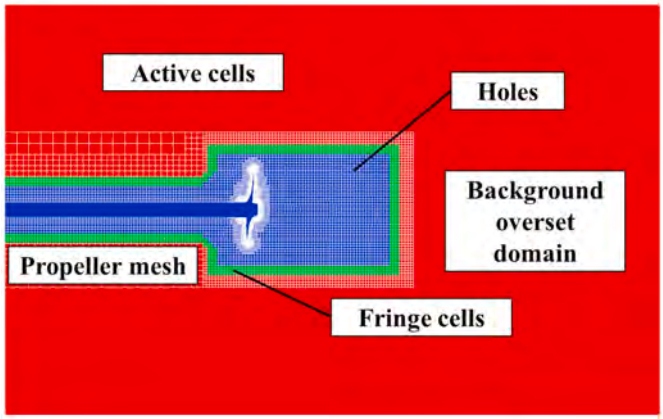

Fig. 1. Background overset domain marking (longitudinal section).

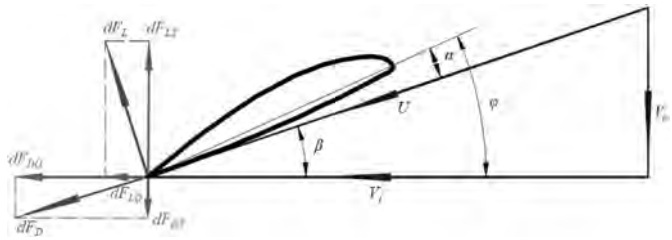

Fig. 2. Velocity and force of blade element.

Then, the accuracy of the improved AAD-BEMT model under the non-uniform flow state is verified by KCS ship self-propulsion test, where the unstructured overset grid is accounted for ship motion. Three different propeller models, i.e., the discretized propeller model based on the overset grid method, the traditional descriptive body-force HO model, and the improved AAD-BEMT model are used for the ship self-propulsion simulation. The radial load distribution and the wake velocity distribution of the propeller are compared and discussed in order to focus on the ability of the proposed AAD-BEMT model to reflect the discretized propeller momentum transport.

The framework of this paper is structured as follows: Section 2 provides details of the numerical methods which followed by the calculation conditions given in Section 3. The numerical results and discussions are presented in Section 4. Finally, the conclusions are drawn in Section 5.

2. Numerical methods

2.1. naoe-FOAM-os-SJTU solver

In this study, the object in open-water tests by the body-force model is only the propeller shaft, so the static grid can meet the simulation requirements. For the open-water test by the discretized propeller, ship resistance test, and ship self-propulsion test, the inhouse CFD solver naoe-FOAM-os-SJTU (Wang et al., 2019) is used. The solver is a viscous multiphase flow overset mesh solver, which was developed based on the open-source platform OpenFOAM. It includes a six-degree-of-freedom motion system, so it is very convenient to handle the rotation of the propeller. naoe-FOAM-os-SJTU solver inherits the finite volume method and numerical schemes of OpenFOAM and uses the PIMPLE algorithm - a combination of Pressure-Implicit with Splitting of Operators (PISO) algorithm and Semi-Implicit Method for Pressure Linked Equations (SIMPLE) algorithm - to decouple velocity and pressure. For the incompressible viscous fluid, the N–S equation used to solve the flow field is given as:

$$\nabla \cdot \mathbf{U} = 0 \tag{1}$$

$$\frac{\partial \rho \mathbf{U}}{\partial t} + \nabla \cdot \left(\rho(\mathbf{U}-\mathbf{U}_g)\mathbf{U}\right) = -\nabla p_d - \mathbf{g}\cdot\mathbf{x}\nabla\rho + \nabla\cdot\left(\mu_{eff}\nabla\mathbf{U}\right) + (\nabla\mathbf{U})\cdot\nabla\mu_{eff} + f_\sigma + (f_\varepsilon)_i \tag{2}$$

where p is the pressure, ρ is the density, $\mathbf{U}$ is the fluid velocity, $\mathbf{U}_g$ is the grid velocity and $\mathbf{g}$ indicates the gravity acceleration; $\mu_{eff} = \rho(\nu + \nu_t)$ is the effective viscosity coefficient and $p_d = p\text{-}\rho\mathbf{g}\cdot\mathbf{x}$ denotes the dynamic pressure. As for the numerical simulation of the propeller open-water test, it has not been decided what is the most suitable turbulence model yet (Tu, 2019). In this paper, the k-ω shear stress transport (SST) model has been used. This turbulence model can activate different calculation methods of turbulence parameters based on the variation of the distance from the wall surface. Detailed theories and equations can be obtained in Menter (1994). $(f_\varepsilon)_i$ is the body-force source term, which is calculated by the body-force code provided separately in the modified solver (Churchfield and Lee, 2013).

In this paper, a phase fraction method with artificial compression (Berberović et al., 2009) is used to capture the evolution of the free surface of a ship model during self-propulsion. The transport equation of phase fraction is:

$$\frac{\partial \alpha}{\partial t} + \nabla\cdot\left[(\mathbf{U}-\mathbf{U}_g)\alpha\right] + \nabla\cdot\left[\mathbf{U}_r(1-\alpha)\alpha\right] = 0 \tag{3}$$

α is the phase fraction between 0 and 1. For different values of phase fraction, it represents the following meanings:

$$\begin{cases} \alpha = 0 & air \\ \alpha = 1 & water \\ 0 < \alpha < 1 & interface \end{cases} \tag{4}$$

In recent years, naoe-FOAM-os-SJTU solver has accumulated more and more experience in dealing with ship hydrodynamic problems, such as ship resistance (Zha et al., 2014, 2015), ship self-propulsion (Shen et al., 2015), ship maneuvering (Wang and Wan, 2018, 2020), and ship seakeeping (Shen and Wan, 2013, 2016; Shen et al., 2014).

2.2. Propeller model

2.2.1. Discretized propeller model

The discretized propeller model (DP) is based on the propeller geometry to generate the propeller boundary grid. By directly considering the effect of the geometry boundary on the fluid, most of the flow field details can be simulated. The key to the application of the discretized propeller model is to deal with the grid motion of propeller geometry. Static grids cannot simulate such problems because the rotational motion destroys the topological relationship between grids. In naoe-FOAM-os-SJTU, the hull, background, and propeller mesh are independent of each other, so the relative motion between any mesh can be carried out without constraints.

Before the simulation is performed, each grid is "marked" to determine its role in information transfer between overset domain and mesh, as shown in Fig. 1. The detailed principle can refer to Shen et al. (2015).

The grid coordinate motion of the propeller is calculated by using Eq. (5):

$$\mathbf{x}^n_{prop} = \begin{bmatrix} c+n_1^2(1-c) & n_1n_2(1-c)-n_3s & n_1n_1(1-c)+n_2s \\ n_1n_2(1-c)+n_3s & c+n_2^2(1-c) & n_2n_3(1-c)-n_1s \\ n_1n_3(1-c)-n_2s & n_2n_1(1-c)+n_1s & c+n_3^2(1-c) \end{bmatrix} \left(\mathbf{x}^0_{prop} - \mathbf{p}_a\right) + \mathbf{p}_a \tag{5}$$

Where $c = \cos\alpha$, $s = \sin\alpha$; $\mathbf{n} = (n_1, n_2, n_3)$ is the unit vector through the propeller shaft, $\mathbf{P}_a$ is a point on the shaft of the propeller; x^0_{prop} and x^n_{prop} are the initial position and the position after the rotating of propeller mesh. When the propeller mesh rotates to the next time-step, the new

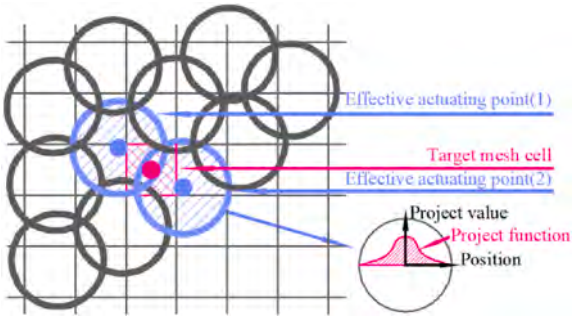

Fig. 3. Gaussian projection scheme.

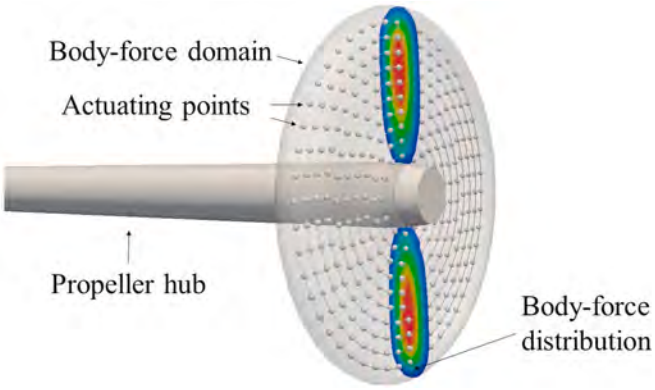

Fig. 4. Diagram of the actuating points' distribution.

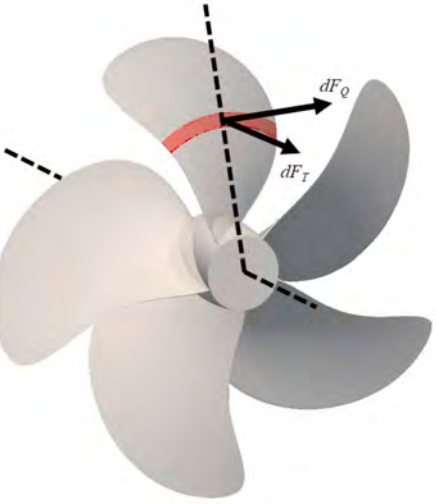

Fig. 5. Diagram of the propeller blade element.

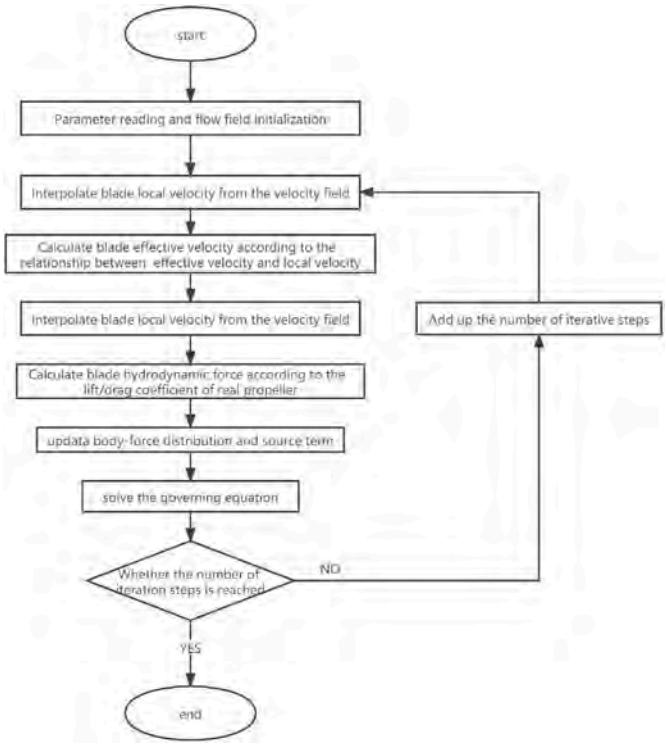

Fig. 6. Flowchart of the AAD-BEMT solver.

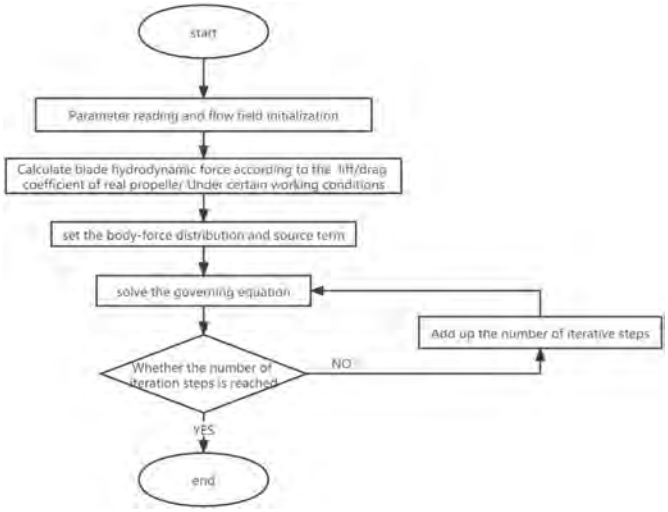

Fig. 7. Flowchart of the AAD solver.

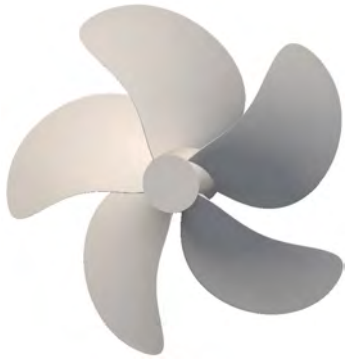

Fig. 8. Geometry of the KP505 propeller.

Fig. 9. Geometry of the KCS ship.

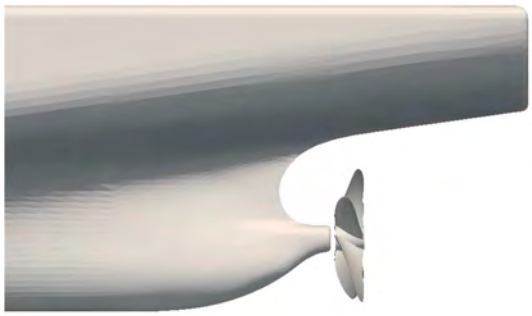

Fig. 10. Position of the KP505 propeller.

Table 1
Principal dimension of the KCS ship.

Main particulars	symbol	Model scale	Full scale
Scale factor	λ	31.6	–
Length between perpendiculars	L_{pp}(m)	7.2786	230
Length of waterline	L_{wL}(m)	7.3576	232.5
Maximum beam of waterline	B_{wL}(m)	1.019	32.2
Draft	T(m)	0.342	10.8
Displacement	Δ (m^2)	1.649	52030
Wetted area without rudder	A_w(m^2)	9.4376	9424
Block coefficient	C_B(m)	0.6505	0.6505
Longitudinal center of buoyancy, fwd+	LCB(%L_{PP})	−1.48	−1.48
Vertical center of gravity (from keel)	KG(m)	0.230	7.28
Moment of inertia	K_{yy}/L_{PP}	0.25	0.25

Table 2
Principal dimension of the KP505 propeller.

Main particulars	symbol	Model scale	Full scale
Scale factor	λ	31.6	–
Diameter	D(m)	0.25	7.9
Mean pitch ratio	P_{mean}/D	0.95	0.95
Area ratio	A_e/A_0	0.800	0.800
Hub ratio	d_h/D	0.180	0.180
Number of blades	Z	5	5
Section profile	–	NACA66	NACA66

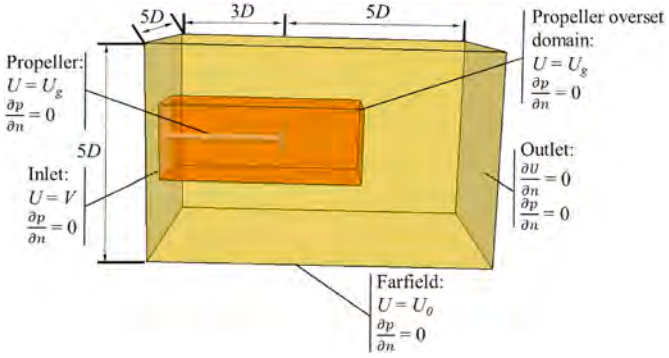

Fig. 11. Computational domain of the discretized propeller model.

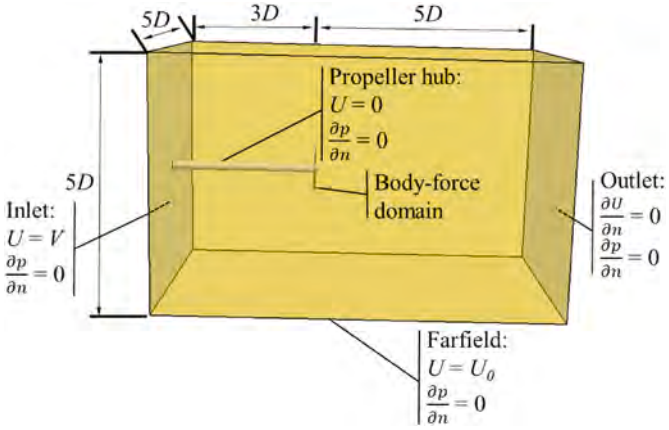

Fig. 12. Computational domain of the body-force propeller model.

grid topological relationship is calculated by Domain Connectivity Information (DCI) to solve the dynamic mesh problem of the propeller.

2.2.2. AAD-BEMT body-force model

BEMT is one of the iterative body-force models, which will iteratively calculate propeller load according to the inflow distribution. In this paper, the geometric AOA is used to calculate the hydrodynamic performance of the blade element as shown in Fig. 2.

In blade coordinates, the equation for calculating thrust and torque of blade element is:

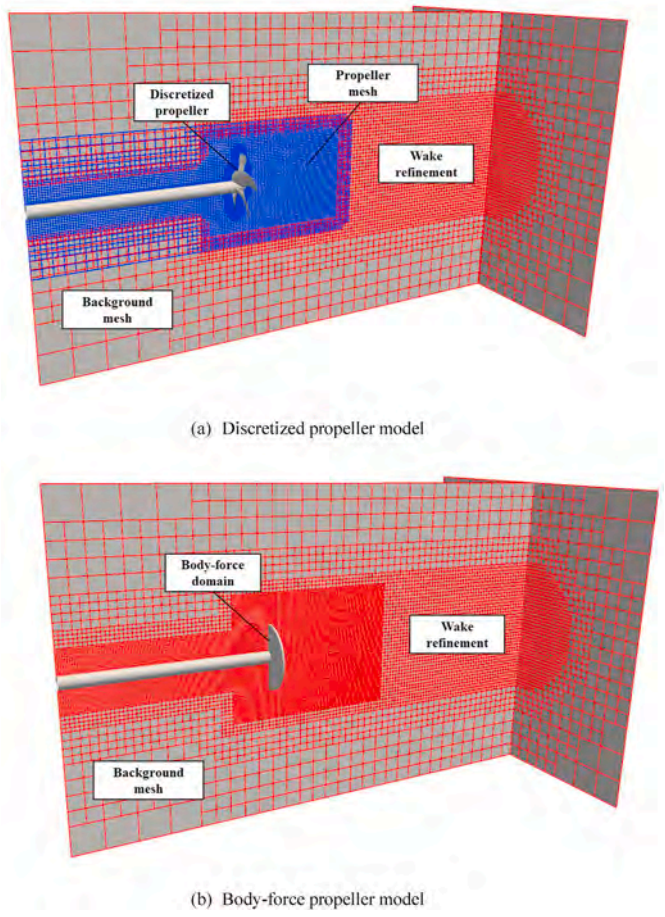

Fig. 13. Mesh refinement of propeller open-water test by different propeller model.

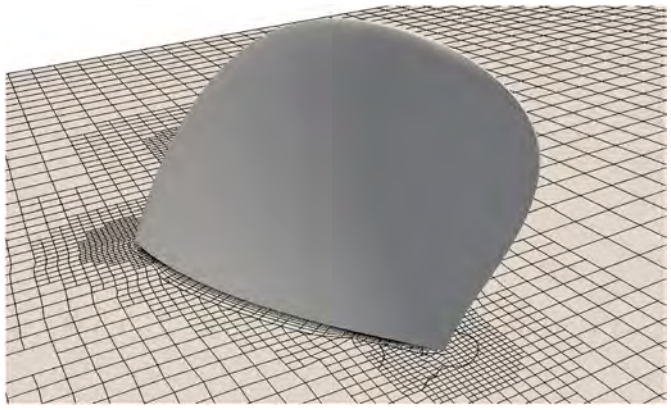

Fig. 14. Propeller boundary layer.

Table 3
The mesh number in different overset domain.

	background	hull	propeller
mesh number (M)	0.71	0.82	1.48

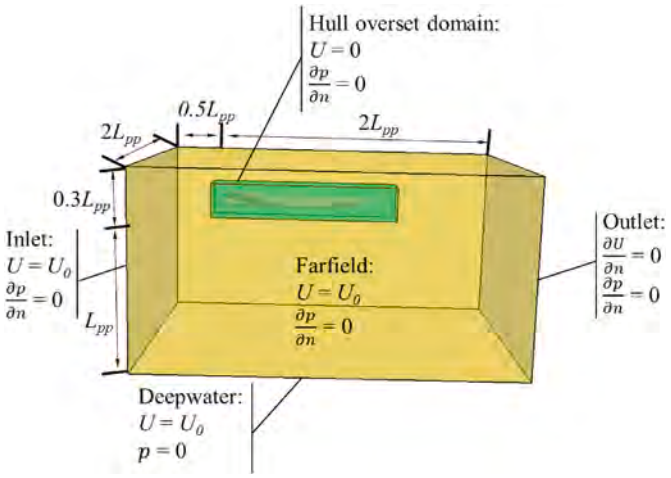

Fig. 15. Computational domain of the KCS ship resistance test.

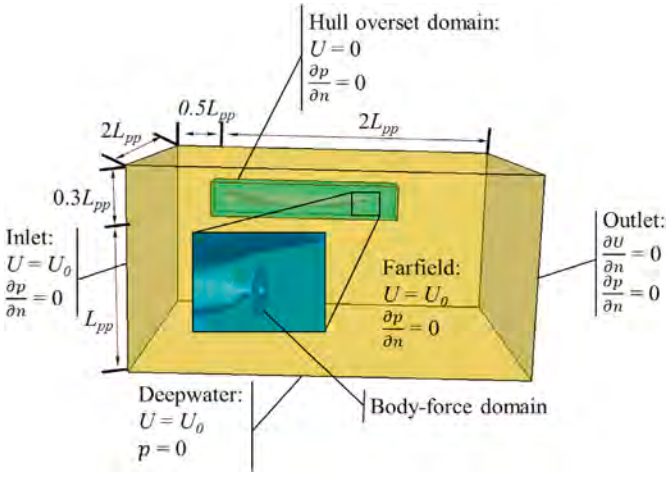

Fig. 16. Computational domain of the KCS ship self-propulsion test (body-force propeller model).

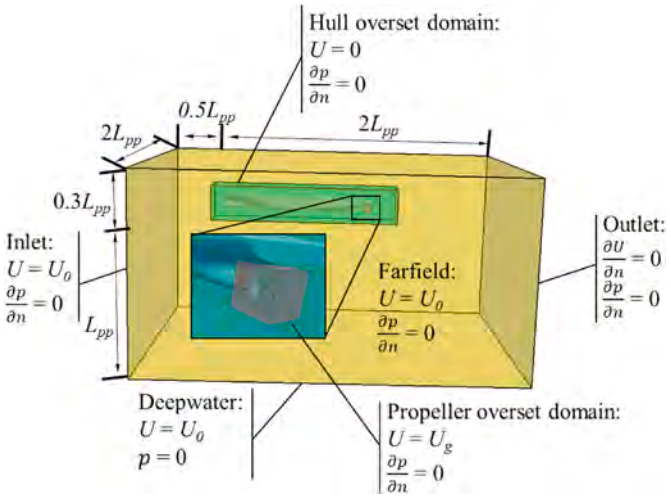

Fig. 17. Computational domain of the KCS ship self-propulsion test (discretized propeller model).

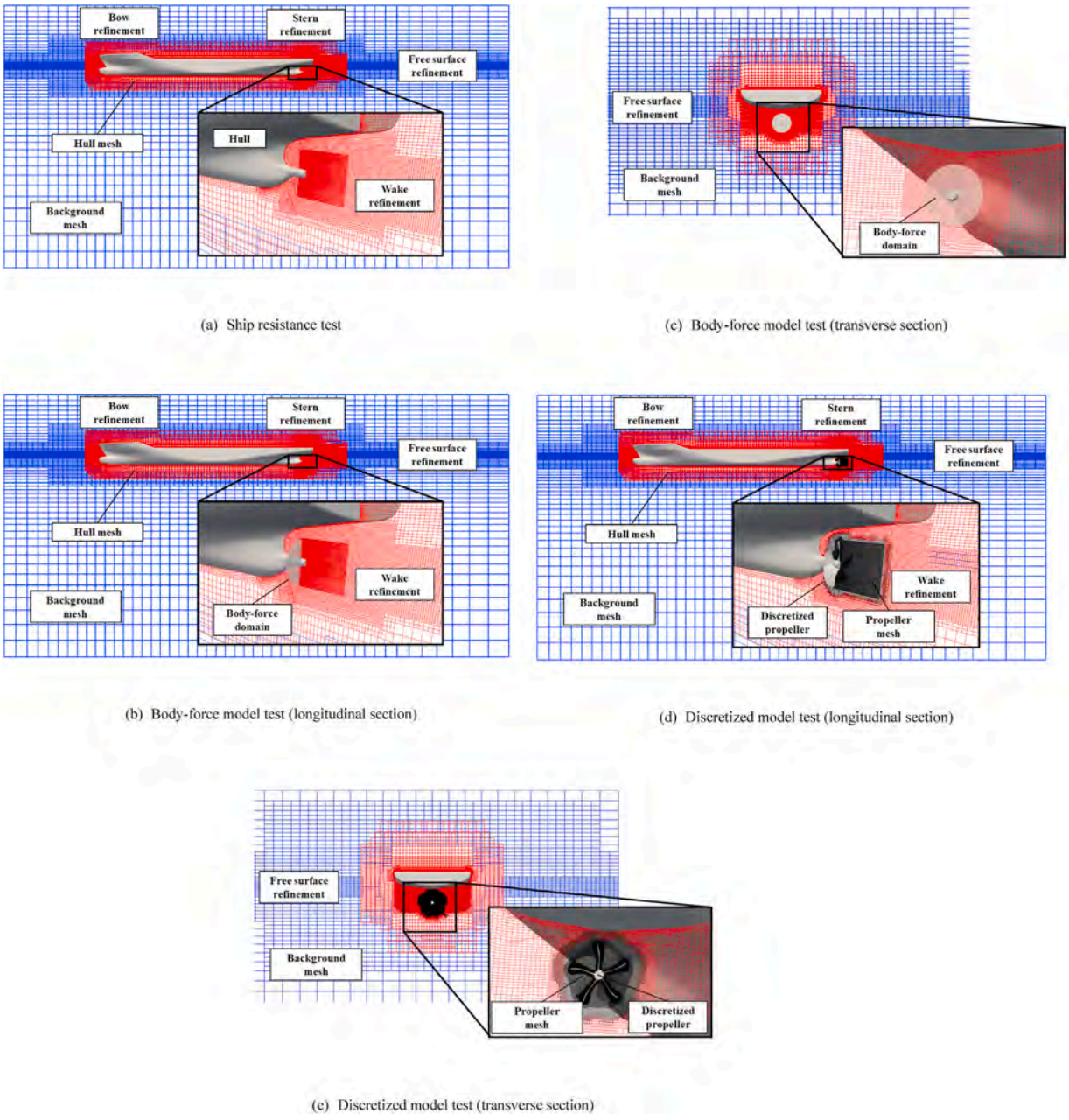

Fig. 18. Mesh refinement of the ship resistance test and the ship self-propulsion test.

Table 4
Mesh convergence study of the KP505 body-force model open-water test.

Case name	ID	Mesh size(M)	K_T	Error (%)	K_Q	Error (%)	η	Error (%)
EFD		–	0.185	–	0.0311	–	0.665	–
Coarse	S_1	0.22	0.176	−4.86%	0.0301	−3.22%	0.651	−2.04%
Medium	S_2	0.59	0.183	−1.30%	0.0309	−0.66%	0.658	−0.99%
Fine	S_3	1.51	0.185	0.22%	0.0312	0.33%	0.662	−0.45%
R_G	–	–	0.4274	–	0.3863	–	0.5112	–
P_G	–	–	2.4525	–	2.7443	–	1.9363	–
$\delta_{RE}(\%S_D)$	–	–	1.1371	–	0.6226	–	0.5615	–
$U_G(\%S_D)$	–	–	1.9094	–	1.8678	–	1.6846	–
Convergence type	–	–	Monotonic	–	Monotonic	–	Monotonic	–

Table 5
Mesh convergence study of the KP505 Discretized propeller model open-water test.

Case name	ID	Mesh size(M)	K_T	Error (%)	K_Q	Error (%)	η	Error (%)
EFD		–	0.185	–	0.0311	–	0.665	–
Coarse	S_1	0.50	0.194	5.09%	0.0324	4.22%	0.668	0.49%
Medium	S_2	1.22	0.184	−0.27%	0.0311	−0.11%	0.662	−0.51%
Fine	S_3	3.18	0.185	0.00%	0.0310	−0.28%	0.665	−0.06%
R_G	–	–	−0.0507	–	0.0403	–	−0.4455	–
P_G	–	–	–	–	9.2635	–	–	–
$\delta_{RE}(\%S_D)$	–	–	–	–	−0.0073	–	–	–
$U_G(\%S_D)$	–	–	2.6812	–	0.3414	–	0.5003	–
Convergence type	–	–	Oscillatory	–	Monotonic	–	Oscillatory	–

Table 6
Mesh convergence study of the KCS model resistance test.

Case name	ID	Mesh size(M)	C_p	Error (%)	C_v	Error (%)	C_t	Error (%)	w	Error (%)
EFD		–	7.18E-04	–	2.83E-03	–	3.55E-03	–	0.686	
Coarse	S_1	0.60	7.83E-04	9.01%	2.84E-03	0.20%	3.62E-03	1.92%	0.648	−5.54%
Medium	S_2	1.53	7.26E-04	1.08%	2.75E-03	−2.91%	3.47E-03	−2.16%	0.668	−2.62%
Fine	S_3	3.80	7.23E-04	0.73%	2.81E-03	−0.79%	3.53E-03	−0.54%	0.674	−1.75%
R_G	–	–	0.0444	–	−0.6828	–	−0.3972	–	0.2970	–
P_G	–	–	8.9879	–	–	–	–	–	3.5034	–
$\delta RE(\%S_D)$	–	–	−0.0163	–	–	–	–	–	0.3664	–
$U_G(\%S_D)$	–	–	0.6877	–	1.5554	–	2.0421	–	1.3687	–
Convergence type	–	–	Monotonic	–	Oscillatory	–	Oscillatory	–	Monotonic	–

Table 7
Time step convergence study of the KP505 Discretized propeller model open-water test.

Case name	ID	Time- step(s)	K_T	Error (%)	K_Q	Error (%)	η	Error (%)
EFD		–	0.185	–	0.0311	–	0.665	–
Coarse	S_1	0.001	0.184	−0.38%	0.0309	−0.52%	0.664	−0.21%
Medium	S_2	0.0005	0.184	−0.29%	0.0311	−0.11%	0.662	−0.52%
Fine	S_3	0.00025	0.185	−0.26%	0.0311	0.02%	0.661	−0.62%
R_T	–	–	0.3712	–	0.3284	–	0.3141	–
P_T	–	–	1.4295	–	3.2133	–	3.3416	–
$\delta RE(\%S_D)$	–	–	0.0202	–	0.0652	–	−0.0452	–
$U_G(\%S_D)$	–	–	0.0377	–	0.2945	–	0.2299	–
Convergence type	–	–	Monotonic	–	Monotonic	–	Monotonic	–

Table 8
Time step convergence study of the KCS resistance test.

Case name	ID	Time- step(s)	C_p	Error (%)	C_v	Error (%)	C_t	Error (%)	w	Error (%)
EFD		–	7.18E-04	–	2.83E-03	–	3.55E-03	–	0.686	
Coarse	S_1	0.001	7.29E-04	1.55%	2.74E-03	−3.11%	3.47E-03	−2.22%	0.669	−2.49%
Medium	S_2	0.0005	7.27E-04	1.21%	2.76E-03	−2.33%	3.49E-03	−1.67%	0.669	−2.48%
Fine	S_3	0.00025	7.26E-04	1.14%	2.76E-03	−2.34%	3.49E-03	−1.69%	0.669	−2.43%
R_G	–	–	0.2066	–	−0.0157	–	−0.0429	–	15.9354	–
P_G	–	–	2.2751	–	–	–	–	–	–	–
$\delta RE(\%S_D)$	–	–	−0.0181	–	–	–	–	–	–	–
$U_G(\%S_D)$	–	–	0.0283	–	−0.3922	–	−0.2786	–	−0.0015	–
Convergence type	–	–	Monotonic	–	Oscillatory	–	Oscillatory	–	Oscillatory	–

$$U = \sqrt{V_t^2 + V_a^2} \tag{6}$$

$$\beta = \tan\frac{V_a}{V_t} \tag{7}$$

$$\alpha = \phi - \beta \tag{8}$$

$$dF_L = \frac{1}{2}\rho C_L U^2 c_r dr \tag{9}$$

$$dF_D = \frac{1}{2}\rho C_D U^2 c_r dr \tag{10}$$

$$dF_T = dF_{LT} - dF_{DT}, dF_{LT} = dF_L\cos\beta, dF_{DT} = dF_D\sin\beta \tag{11}$$

$$dF_Q = (dF_{LQ} + dF_{DQ})r, dF_{LQ} = dF_L\sin\beta, dF_{DQ} = dF_D\cos\beta \tag{12}$$

where V_t and V_a are the axial and tangential effective inflow velocity, respectively. α is the geometric AOA, β is the hydrodynamic pitch Angle, φ is the blade element pitch angle, dF_L and dF_D is the blade element lifting/drag force, dF_T and dF_Q are the contribution of blade element to thrust and torque, dF_{LT}, dF_{DT}, dF_{LQ} and dF_{DQ} are the projections of lifting/drag force in axial and tangential directions, respectively.

To improve the accuracy of the BEMT propeller model, the accurate calculation of blade element force coefficient and AOA should be ensured. The force coefficient of the blade element can be calculated by discretized propeller model open-water CFD results, and the AAD is to ensure the accuracy of the calculation of AOA. The effective AOA under

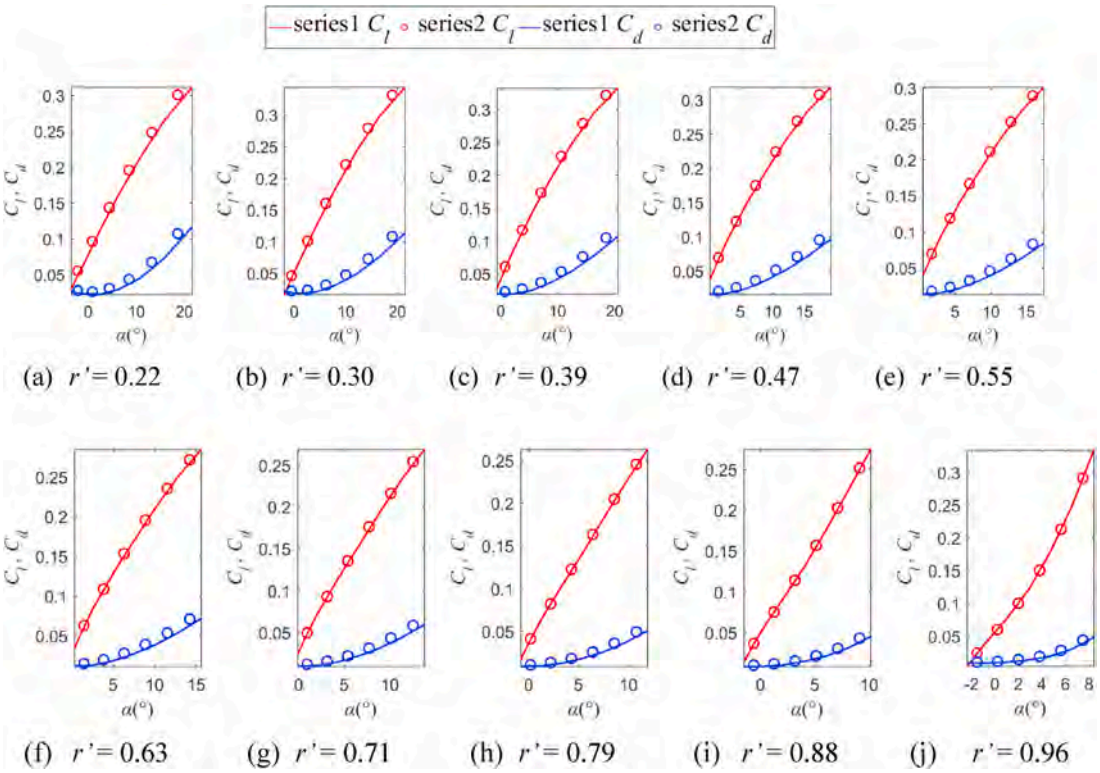

Fig. 19. Blade element force coefficient under the two sets of working conditions.

Table 9
Error of Cl/Cd interpolation.

	r' = 0.22	r' = 0.30	r' = 0.39	r' = 0.47	r' = 0.55	r' = 0.63	r' = 0.71	r' = 0.79	r' = 0.88	r' = 0.96
J = 0.45	3.45%	3.24%	2.52%	2.01%	1.68%	1.46%	1.28%	1.07%	0.80%	0.09%
J = 0.55	3.19%	3.26%	2.69%	2.21%	1.85%	1.58%	1.35%	1.12%	0.80%	0.01%
J = 0.65	3.81%	3.92%	3.31%	2.79%	2.38%	2.07%	1.76%	1.48%	1.15%	0.33%
J = 0.75	3.69%	3.95%	3.35%	2.81%	2.37%	2.01%	1.72%	1.42%	0.91%	0.03%
J = 0.85	3.14%	3.80%	3.30%	2.34%	1.72%	1.23%	0.88%	0.51%	0.09%	0.75%
J = 0.95	3.50%	3.45%	3.78%	1.69%	1.97%	1.46%	1.90%	1.51%	1.36%	0.19%

the action of airfoil and source term will be different, so this paper defines the blade element performance by the geometric AOA, which needs to obtain the inflow velocity of the blade element. However, for non-uniform inflow conditions such as the behind-ship condition, the inflow of the propeller is unknown, and the body-force model can only input the flow field information in the action area. Therefore, it is necessary to deduce the inflow through the local velocity, that is, to establish the relationship between the local velocity and the inflow velocity of the blade element under the action of the source term.

In this paper, the actuating point represents the position of the propeller blade element. The blade load is obtained by the hydrodynamic force calculation of the blade element, which is mapped to the grid of the computational domain via a certain projection function. Each actuating point has a spherical effective range. Fig. 3 shows the projection scheme of actuating point. The red area represents the target grid and its center, while the blue circle represents the effective actuating point and its effective range around the grid. When the center of the grid is within the effective range of an actuating point, the weight of the actuating point to the grid source item is calculated by the Gaussian projection function:

$$\eta_\varepsilon(d) = \frac{1}{\varepsilon^3 \pi^{3/2}} \exp\left[-\left(\frac{d_i}{\varepsilon}\right)^2 \right] \tag{13}$$

where ε is the effective projection distance ($\varepsilon = 0.01$m in this study). The value of the source term in the center of the grid is the sum of the contributions from all the surrounding effective actuation points.

The region of body-force is an envelope region formed by the projection region of a series of excitation points. In this paper, the distribution of the actuating points is designed as a disc, corresponding to the large surface ratio of the marine propeller. The spacing of the actuating points is equal in the radial and circumferential directions. There is only one layer along the axial direction, as shown in Fig. 4. The position of the actuating point is constant relative to the hull during the calculation.

Because of the difference between the airfoil and the source term on local velocity, the velocity relationship is obtained by using an AAD. AAD is a descriptive propeller body-force model, but it is not directly involved in the problem of flow field simulation study. It provides the information on the flow field under the action of the source term for the BEMT propeller model. In this way, the blade element can maintain the same accuracy as the descriptive body-force model. At the same time, the accuracy of the model and the ability to deal with complex problems can be guaranteed because the calculation of blade elements is not coupled with each other.

The parameters used to record the relationship between local velocity and inflow velocity of blade element should meet the following conditions: Firstly, for the same propeller with the same advance ratio, these parameters should be the same to meet the similarity law of the

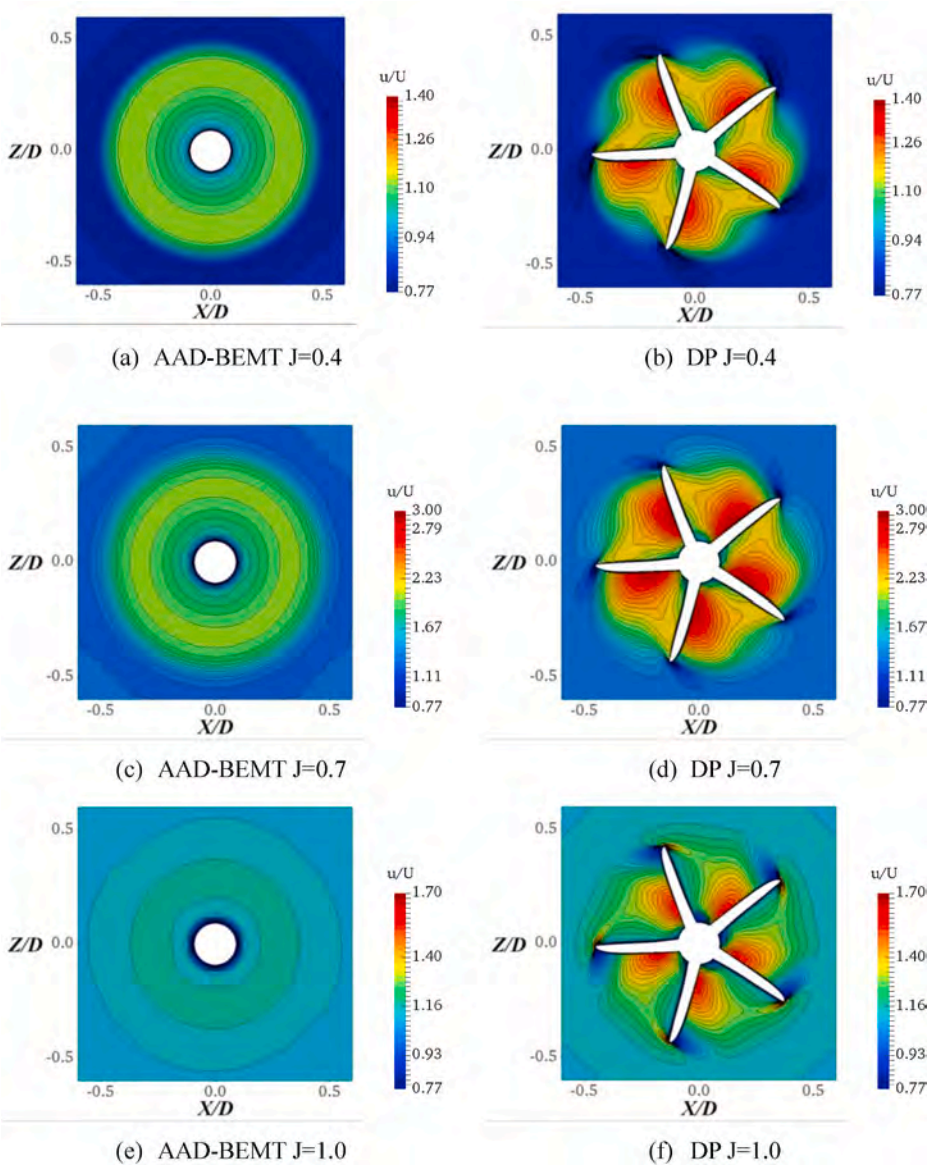

Fig. 20. Comparation of local flow field in propeller plane of the AAD and the discretized propeller model.

model. Secondly, the definition of parameters and the data sampling method should be simple, while the data sampling result should be uncontroversial. Thirdly, the corresponding relationship between parameters can be established to allow the flow velocity can be calculated according to the local velocity in solving process. Lastly, the model can iterate to a stable state according to the initial condition, and correctly simulate the load distribution of the propeller under corresponding working conditions. Based on this, the following dimensionless blade element velocity parameters are selected in this paper to represent the velocity relationship:

$$V_a^{'} = \frac{V_a}{nD} \tag{14}$$

$$V_t^{'} = \frac{V_t}{V_x} \tag{15}$$

$$V_x^{'} = \frac{V_x}{nD} \tag{16}$$

$$V_\theta^{'} = \frac{V_\theta}{V_x} \tag{17}$$

For condition 1, due to geometric similarity, the velocity ratios of any two points in the flow field in any direction are the same value for the same advance ratio. Therefore, V/V_x, V_t/V_x and V_θ/V_x do not change with the advance velocity coefficient, that is, the selected parameters meet the similarity law.

For condition 2, since the open-water flow field of the AAD is circumferentially uniform, the local velocity of the blade element can be obtained from the position of the actuating point by flow field interpolation, as shown in Fig. 4. This method avoids the complexity of obtaining local velocity from discretized propeller model.

For condition 3, the data collection of the AAD was based on open-water simulations with different advance ratios. Velocity sampling results obtained from the AAD are arranged into the following vector form:

$$\mathbf{V}_\mathbf{a}^{'} = \left[V_{a,AAD,1}^{'}, V_{a,AAD,2}^{'}, \ldots V_{a,AAD,i}^{'}\right] \tag{18}$$

$$\mathbf{V}_\mathbf{x}^{'}(r^{'}) = \left[V_{x,AAD,1}^{'}(r^{'}), V_{x,AAD,2}^{'}(r^{'}), \ldots V_{x,AAD,i}^{'}(r^{'})\right] \tag{19}$$

$$\mathbf{V}_\mathbf{t}^{'}(r^{'}) = \left[V_{t,AAD,1}^{'}(r^{'}), V_{t,AAD,2}^{'}(r^{'}), \ldots V_{t,AAD,i}^{'}(r^{'})\right] \tag{20}$$

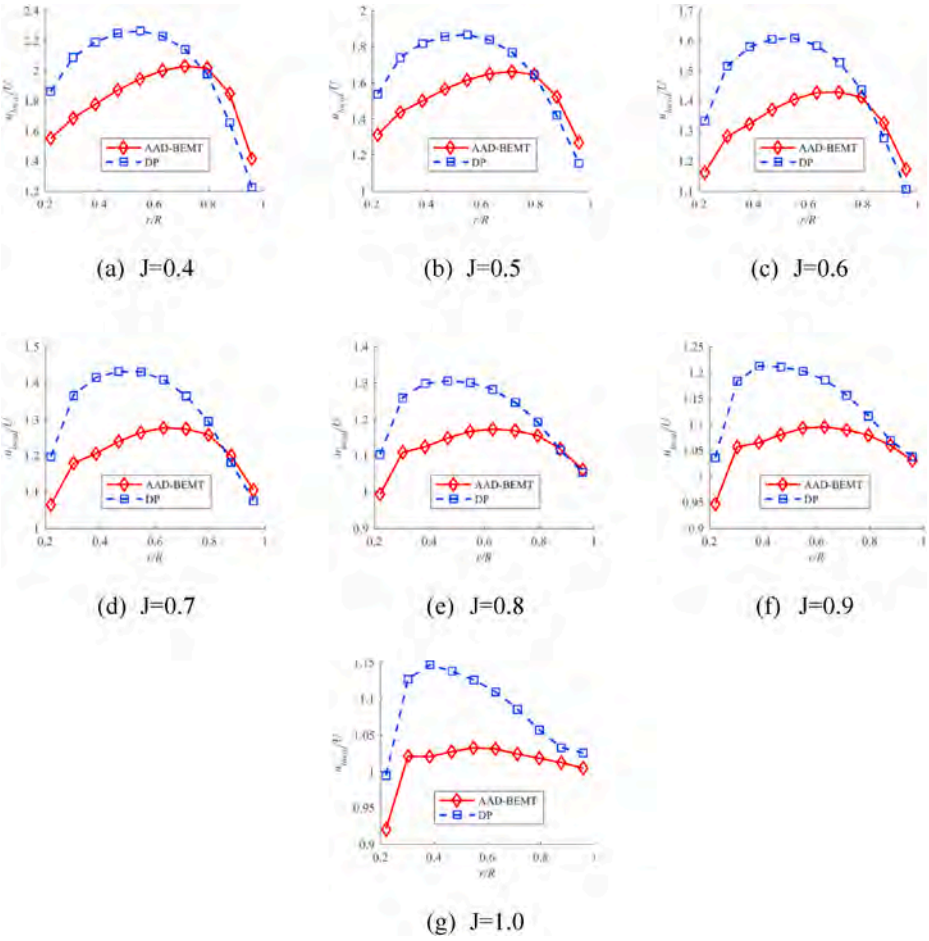

Fig. 21. Comparison of blade element local axial velocity obtained by the AAD and the discretized propeller models.

$$\mathbf{V}_{\boldsymbol{\theta}}^{'}(r^{'})=\left[V_{\theta,AAD,1}^{'}(r^{'}),V_{\theta,AAD,2}^{'}(r^{'}),\ldots V_{\theta,AAD,i}^{'}(r^{'})\right] \tag{21}$$

where the subscript *AAD* indicates that the variable is the velocity field data sampled from AAD, the subscripts $1\sim i$ are the results of the ith simulation, and the variable r' represents different radial positions, which also represents different blade elements.

Since propeller diameter D and propeller speed n at each time-step are determined before each iteration of body-force, axial and tangential inflow velocity can be calculated by reading the local velocity of the flow field in each time-step:

$$V_{a}^{'}=f\left(\mathbf{V}_{\mathbf{a}}^{'},\mathbf{V}_{\mathbf{x}}^{'},V_{x}^{'},r^{'}\right)=\mathbf{V}_{\mathrm{a,i-1}}^{'}\times\frac{V_{x}^{'}-\mathbf{V}_{\mathbf{x}}^{'}(r^{'})_{i}}{\mathbf{V}_{\mathbf{x}}^{'}(r^{'})_{i-1}-\mathbf{V}_{\mathbf{x}}^{'}(r^{'})_{i}}+\mathbf{V}_{\mathbf{a}}^{'}\times\frac{V_{x}^{'}-\mathbf{V}_{\mathbf{x}}^{'}(r^{'})_{i-1}}{\mathbf{V}_{\mathbf{x}}^{'}(r^{'})_{i}-\mathbf{V}_{\mathbf{x}}^{'}(r^{'})_{i-1}},V_{x}^{'}\in\left[\mathbf{V}_{\mathbf{x}}^{'}(r^{'})_{i-1},\mathbf{V}_{\mathbf{x}}^{'}(r^{'})_{i}\right] \tag{22}$$

$$V_{t}^{'}=f\left(\mathbf{V}_{\mathbf{t}}^{'},\mathbf{V}_{\boldsymbol{\theta}}^{'},V_{\theta}^{'},r^{'}\right)=\mathbf{V}_{t,i-1}^{'}\times\frac{V_{\theta}^{'}-\mathbf{V}_{\boldsymbol{\theta}}^{'}(r^{'})_{i}}{\mathbf{V}_{\boldsymbol{\theta}}^{'}(r^{'})_{i-1}-\mathbf{V}_{\boldsymbol{\theta}}^{'}(r^{'})_{i}}+\mathbf{V}_{\mathbf{t}}^{'}\times\frac{V_{\theta}^{'}-\mathbf{V}_{\boldsymbol{\theta}}^{'}(r^{'})_{i-1}}{\mathbf{V}_{\boldsymbol{\theta}}^{'}(r^{'})_{i}-\mathbf{V}_{\boldsymbol{\theta}}^{'}(r^{'})_{i-1}},V_{\theta}^{'}\in\left[\mathbf{V}_{\boldsymbol{\theta}}^{'}(r^{'})_{i-1},\mathbf{V}_{\boldsymbol{\theta}}^{'}(r^{'})_{i}\right] \tag{23}$$

For condition 4, it can be proved that the body-force can converge to the correct load distribution state in the subsequent open-water test.

For the calculation of the force coefficient, this paper obtained the load distribution of the three-dimensional blade element through the CFD open-water test of the propeller and then divided the blade element into 10 parts to calculate the force coefficient, as shown in Fig. 5. The idea is the same as Feng et al. (2020a,b). Because the traditional force coefficient fitting formula is derived based on potential flow theory and many unverified assumptions are applied, the data are transferred through piecewise linear interpolation.

The solver in this paper uses the PIMPLE method to decouple the velocity field from the pressure field. Here, the explicit method is applied to solve the body-force, that is, in each time-step, the velocity field of the previous time-step is first used to solve the velocity field, and then the current time-step velocity field is used to calculate the body-force field. The body-force distribution of the AAD does not change during iteration, while for the BEMT solver, the force iterates with the change of the inflow velocity of the blade element. Fig. 6 and Fig. 7 show the flowcharts of the AAD and the AAD-BEMT solver.

2.2.3. HO body-force model

For the descriptive body-force method, the distribution of the body-force force is treated as a function of the radius. Hough and Ordway (1965) first proposed the calculation method of propeller load distribution based on potential flow theory. To establish the HO model, only the torque coefficient and thrust coefficient of the propeller need to be provided, and the calculations are given as:

$$f_{b,x}=\frac{\rho U^{2}}{L_{pp}}A_{x}r^{*}\sqrt{1-r^{*}} \tag{24}$$

$$f_{b,\theta}=\frac{\rho U^{2}}{L_{pp}}A_{\theta}\frac{r^{*}\sqrt{1-r^{*}}}{(1-Y_{H})r^{*}+Y_{H}} \tag{25}$$

$$r^{*}=\frac{r-R_{H}}{R_{P}-R_{H}} \tag{26}$$

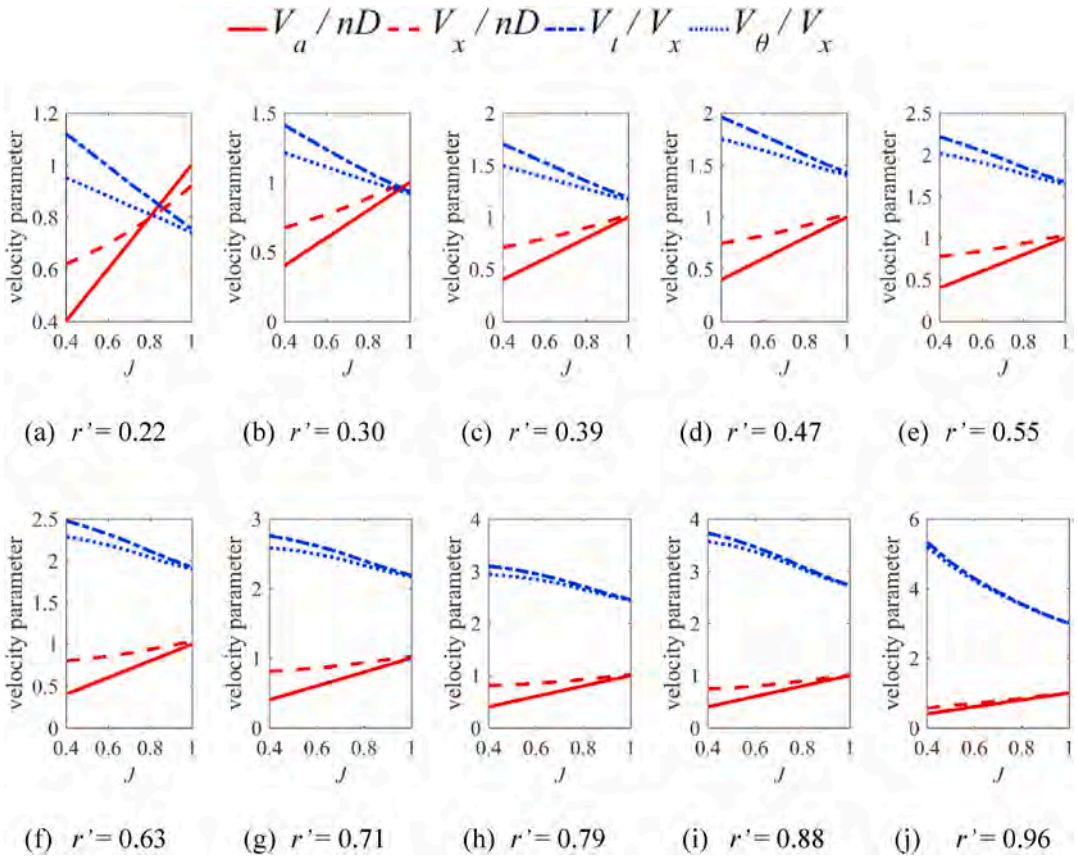

Fig. 22. Blade element velocity parameters in different advance ratios.

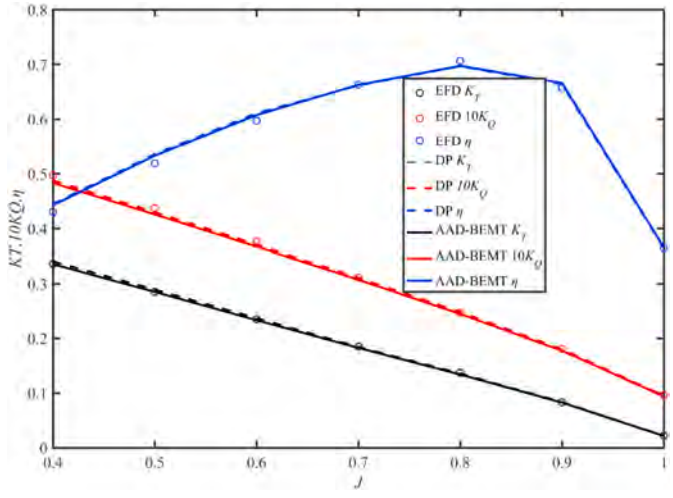

Fig. 23. Comparison of the KP505 propeller open-water curve based on the experiment and different propeller models.

$$Y_H = \frac{R_H}{R_P} \tag{27}$$

$$A_x = \frac{C_t}{\Delta x^*} \frac{105}{16(4+3Y_H)(1-Y_H)} \tag{28}$$

$$A_\theta = \frac{K_Q}{J^2 \Delta x^*} \frac{105}{\pi(4+3Y_H)(1-Y_H)} \tag{29}$$

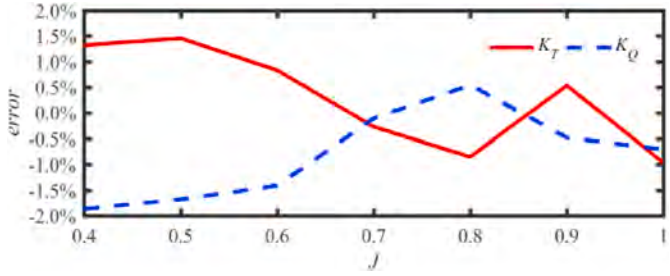

Fig. 24. The error of the discretized propeller model relative to the experiment.

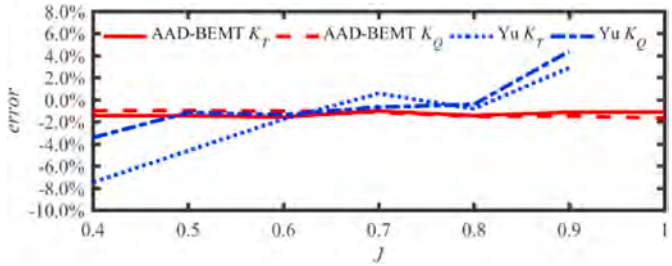

Fig. 25. The error of different body-force propeller model relative to the discretized propeller model.

$$C_t = 32n^2 R_p^2 K_T \Big/ \pi U^2 \tag{30}$$

where $f_{b,x}$ and $f_{b,\theta}$ are the thrust and the torque load per unit volume, respectively, n the propeller rotation speed, r the radial position, R_P and

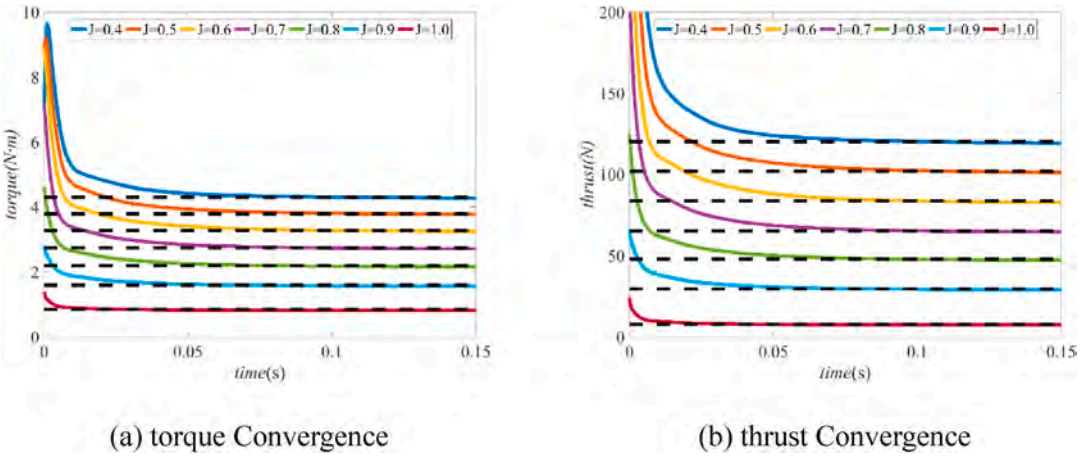

Fig. 26. Convergence process of the AAD-BEMT model.

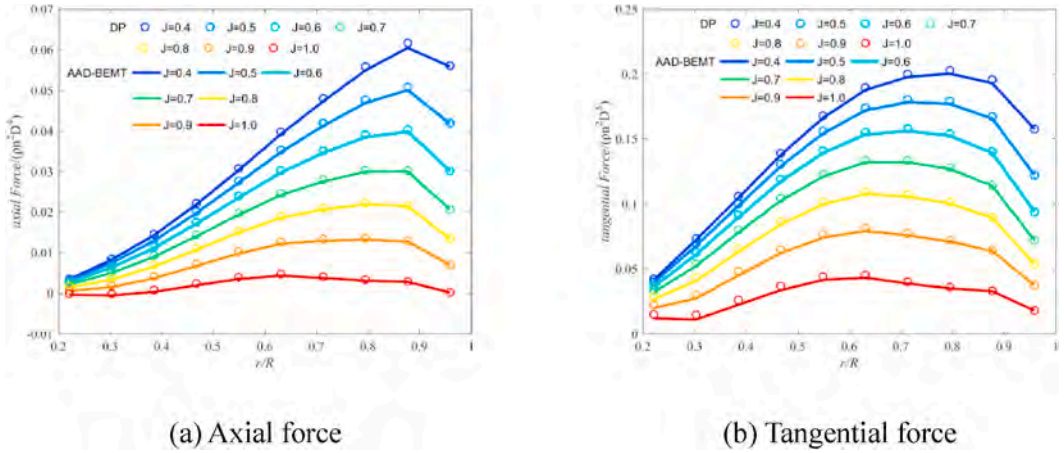

Fig. 27. Comparison of propeller load distributions between the discretized model and the AAD-BEMT model.

R_H indicate the propeller tip radius and the hub radius, respectively. Y_H is the hub diameter ratio, L_{pp} the length between perpendiculars and $\Delta x^* = \Delta x/L_{pp}$ is the dimensionless propeller thickness. In this study, the body-force distribution per unit thickness is applied to calculate the load at the actuating point. J is the velocity coefficient, U is the inflow velocity respectively. K_T and K_Q are the thrust coefficient and the torque coefficient, which are calculated from the open-water curve. Since the propeller inflow is unknown under the behind-hull condition, U is determined by ship speed and wake fraction obtained from the experiment.

3. Computational overviews

3.1. Geometry

In this paper, the KCS ship and the KP505 propeller are selected for the self-propulsion simulation at model scale. Experimental data on the KCS ship can be found from the Tokyo 2005 CFD Workshop (Hino, 2005). Computational models for open-water test, ship resistance test, and ship self-propulsion test are shown in Fig. 8-Fig. 10. The propeller geometry in the ship self-propulsion test is the same as the model in the propeller open-water test. Table 1 and Table 2 show the principal dimension of the model (see Fig. 9).

3.2. Propeller open-water test

The simulation case of the propeller open-water test includes discretized propeller model case and body-force model case. DP case and AAD-BEMT case use the same set of computing grids. The computational domain is a rectangular column with the width and height of 5D and the length of 8D, where the inflow section is 3D. These distances can ensure that the flow field is not affected by the boundary effect. The fluid velocity at the inlet and cylindrical boundary are inflow velocities to simulate the undisturbed condition in the far-field, as shown in Fig. 11 and Fig. 12. The body-force model and the discretized propeller model have the same open-water test grid refinement characteristics, as shown in Fig. 13.

The blocking effect of the hub is considered in the simulation of the body-force model. The body-force is projected at the position of the original blade plane. The thickness spans 6 grids and 15 grids in the radial direction. The Gaussian distance determines the thickness of the projected area, and subsequent studies show that the Gaussian distance set in this paper can make the body-force model take the place of the discretized propeller to simulate momentum transport.

Discretized propeller model uses overset grid technology, and propeller mesh rotates around the propeller shaft at propeller speed. To capture the viscous effect of the blade wall, the boundary layer setting is essential. The propeller boundary layer needs to reach a certain thickness to capture the large gradient flow near the wall. OpenFOAM sets the wall function of ω (Moukalled et al., 2016). For the k-ω SST turbulence model, the height of the first-layer grid should not be too small. Otherwise, to make the grid transition to the size of the far field, a higher grid growth rate or unacceptable boundary layer number are needed, which will greatly reduce the grid quality. Finally, $y_{0.7R}+$ is set to 50, as

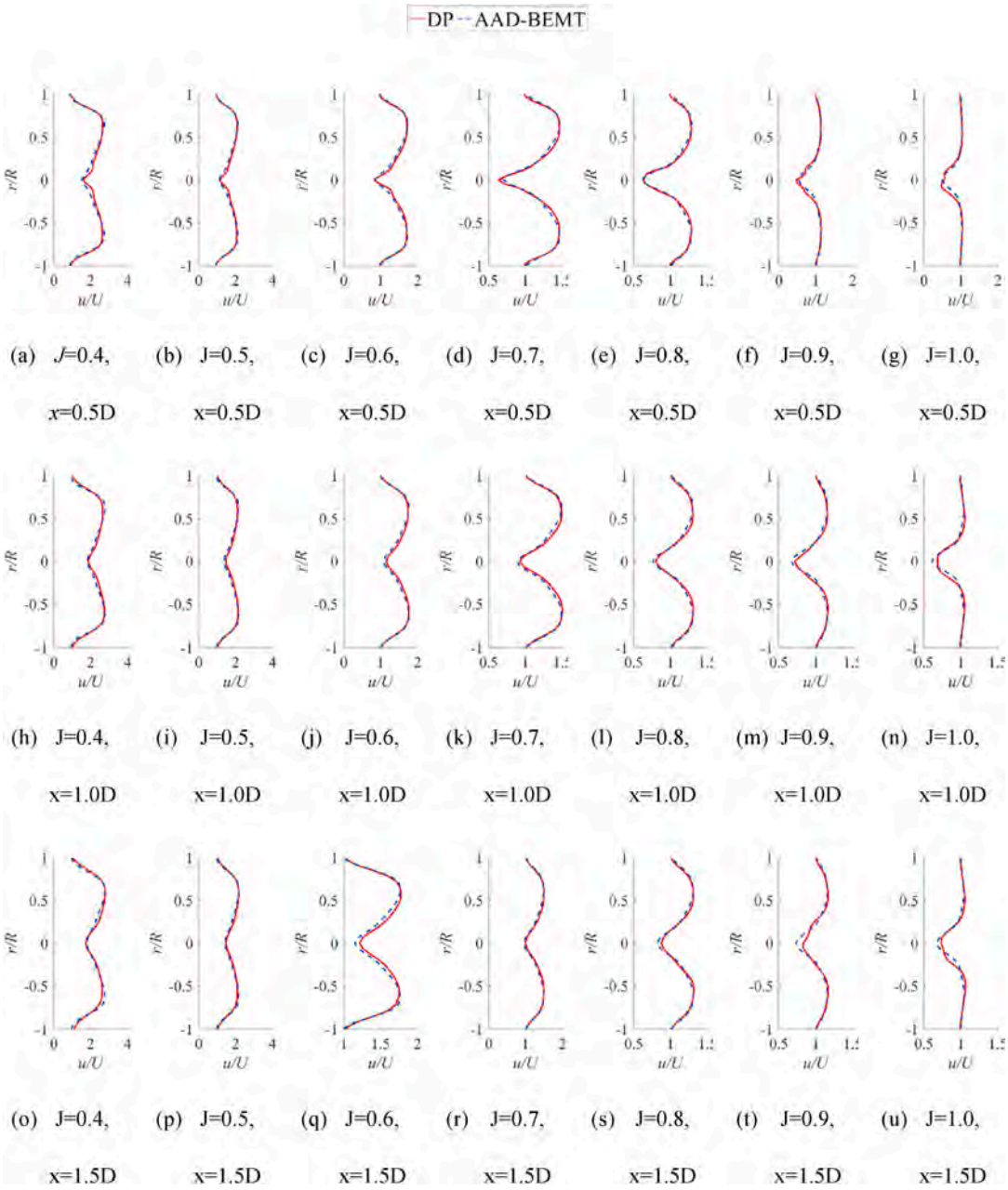

Fig. 28. Comparison of propeller wake between the discretized model and the AAD-BEMT model.

shown in Fig. 14, which can ensure the accuracy of the torque calculation results that greatly affected by the viscous effect.

Due to the time-average consideration of the body-force model, the open-water test based on the body-force model is suitable for the steady-state simulation, while the open-water test based on the discretized propeller model adopts the transient simulation.

3.3. Ship resistance and self-propulsion test

Ship model test includes ship resistance test, body-force model self-propulsion test, and discretized propeller model self-propulsion test. The discretized propeller model self-propulsion test use overset mesh technology which is suitable for simulating the interaction of multiple complex structures. Table 3 shows the mesh number in each mesh region.

In each simulation case, the ship is taken as the reference coordinate system, and the fluid velocity at the bottom, inlet, and both sides of the boundary is the ship velocity. The boundaries are far enough away from the hull that the flow field will not be affected by the waves reflected from the boundary, as shown in Fig. 15-Fig. 17 (see Fig. 16).

Discretized propeller model is used in the discretized propeller self-propulsion test. The propeller hub is considered in the body-force model self-propulsion test, and the position of the blade is the body-force distribution region. The resistance test and body-force model self-propulsion test use the same calculate mesh.

In the body-force model self-propulsion test and the discretized propeller model self-propulsion test, the grid distribution of other positions is the same except for the propeller mesh, as shown in Fig. 18.

The hull mesh and the propeller mesh are generated separately, and the propeller mesh rotates around the shaft according to the preset propeller rotating speed. The purpose of setting the clearance between the hull and the propeller is to provide enough fringe grid for the propeller mesh. The heave and pitch of the hull are not considered in the self-propulsion test, which is the same as the experimental setup. Similar

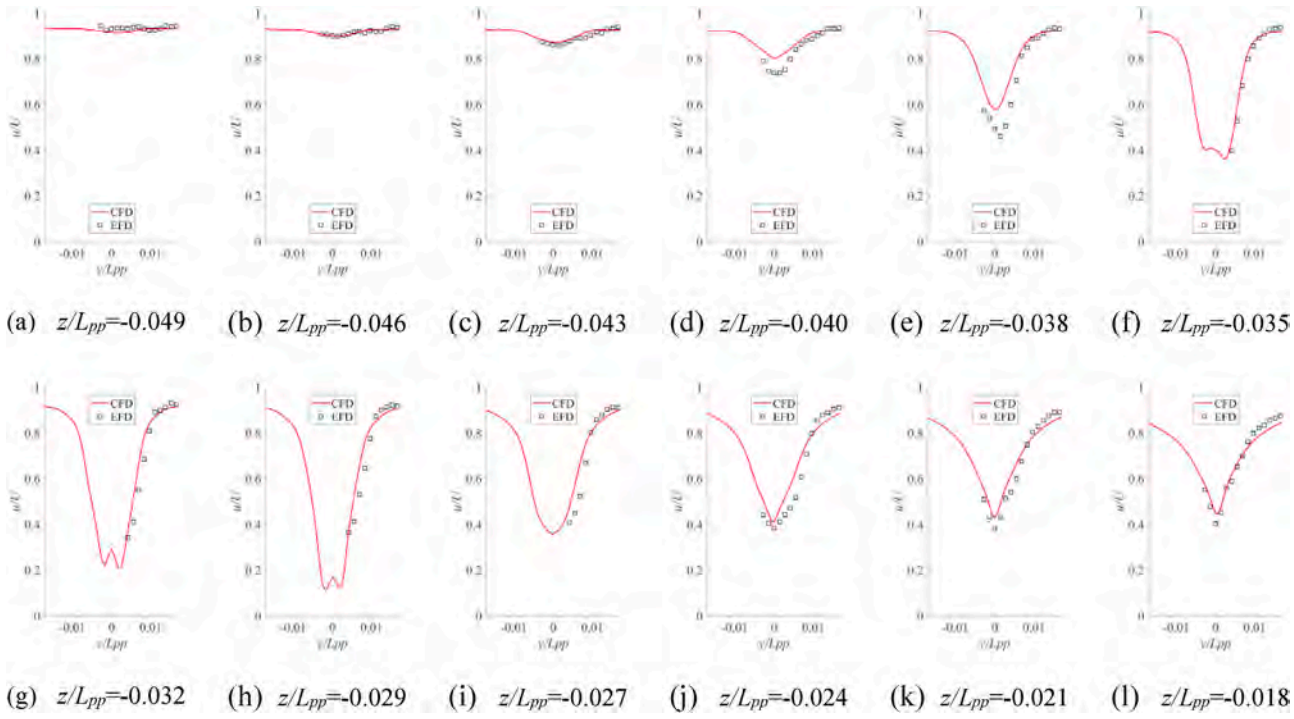

Fig. 29. Comparison of bare hull wakes between the EFD and CFD methods in different slices.

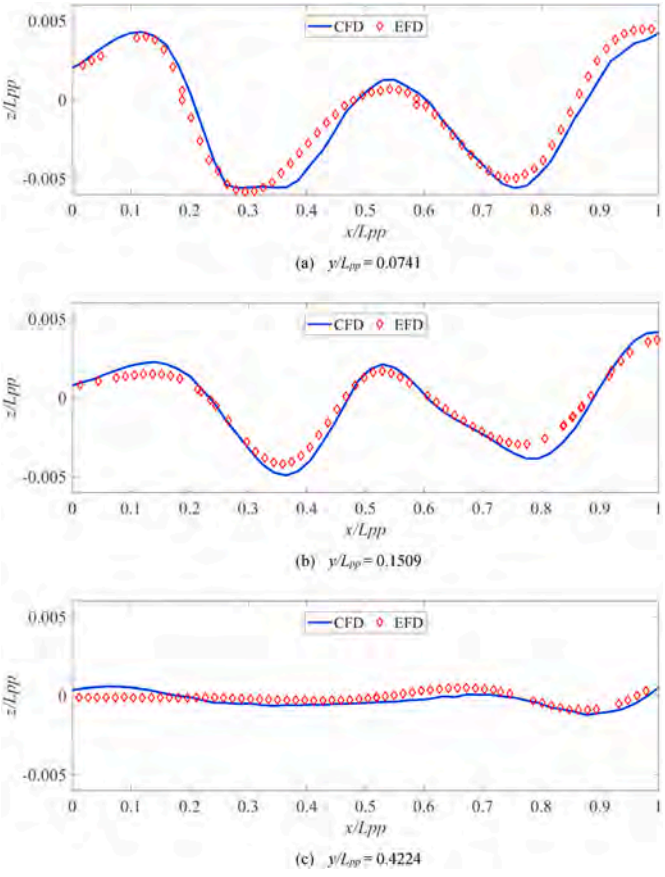

Fig. 30. Comparison of wave heights at different longitudinal sections between the CFD and EFD models.

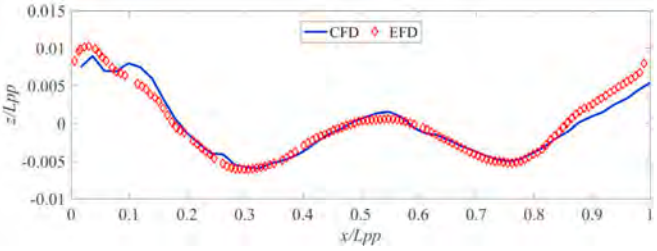

Fig. 31. Comparison of wave height at the ship hull surface.

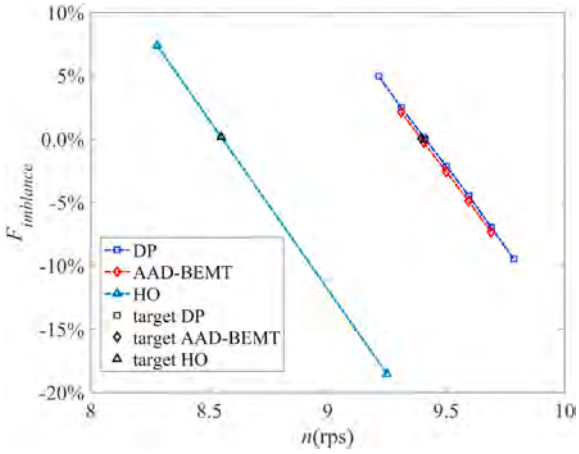

Fig. 32. Force imbalance at different propeller rotation speeds.

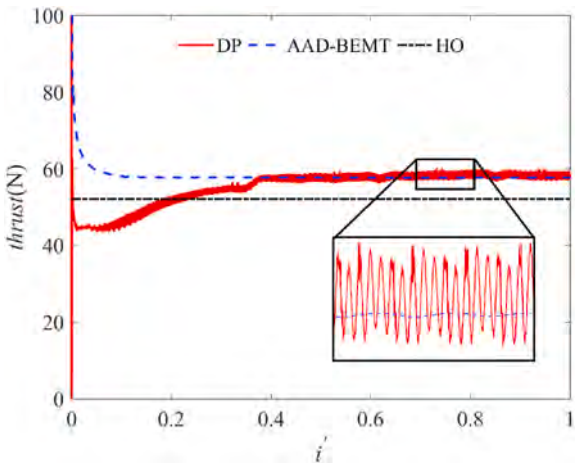

Fig. 33. Thrust convergence process in the self-propulsion test.

to the open-water test, steady-state and transient simulations are used in the ship model self-propulsion test based on the body-force model and the discretized propeller model, respectively.

4. Results and discussion

4.1. CFD validation

Validation and Verification study is carried out to ensure the validity of the simulation parameter settings (Stern et al., 2001; Xing and Stern, 2010). To ensure the validity of the calculated results, the validation and verification of propeller open-water test and ship model resistance test are studied. The key parameters of validation and verification include the error, convergence and uncertainty. For numerical simulation, the most important parameters are the grid size and time-step. The error is defined as follows:

$$E = D - S \tag{31}$$

where D is the result of the physical experiment, and S is the error of

Table 10
KCS ship self-propulsion factor.

	symbol	Experiment	AAD-BEMT	Error	DP	Error	HO	Error
Resistance coefficient	C_T	3.94E-03	3.86E-03	−1.99%	3.89E-03	−1.13%	3.63E-03	−7.98%
Thrust coefficient	K_T	0.170	0.167	−1.70%	0.169	−0.71%	0.183	7.43%
Torque coefficient	K_Q	0.0288	0.0285	−1.17%	0.0287	−0.27%	0.0322	11.76%
Thrust deduction	$1\text{-}t$	0.853	0.844	−1.05%	0.834	−2.18%	0.933	9.32%
Effective wake coefficient	$1\text{-}w_t$	0.792	0.789	−0.44%	0.794	0.20%	0.686	−13.38%
Open-water efficiency	η_0	0.682	0.689	1.01%	0.686	0.64%	0.637	−6.66%
Relative rotative efficiency	η_R	1.011	1.009	−0.21%	1.008	−0.27%	0.956	−5.40%
Advance ratio	J	0.728	0.737	1.27%	0.734	0.80%	0.705	−3.17%
Rate of revolution	n	9.500	9.395	−1.11%	9.41	−0.93%	8.550	−10.00%

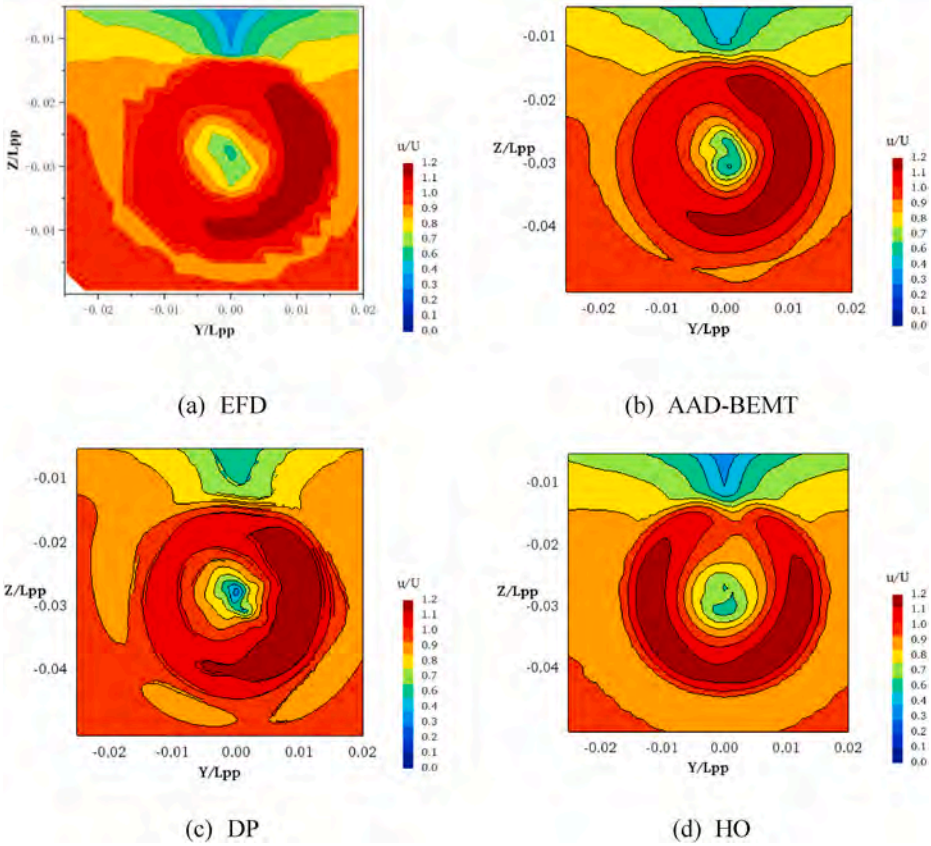

Fig. 34. Ship wake distribution obtained by the EFD and different CFD propeller models ($x/L_{pp} = 0.9911$).

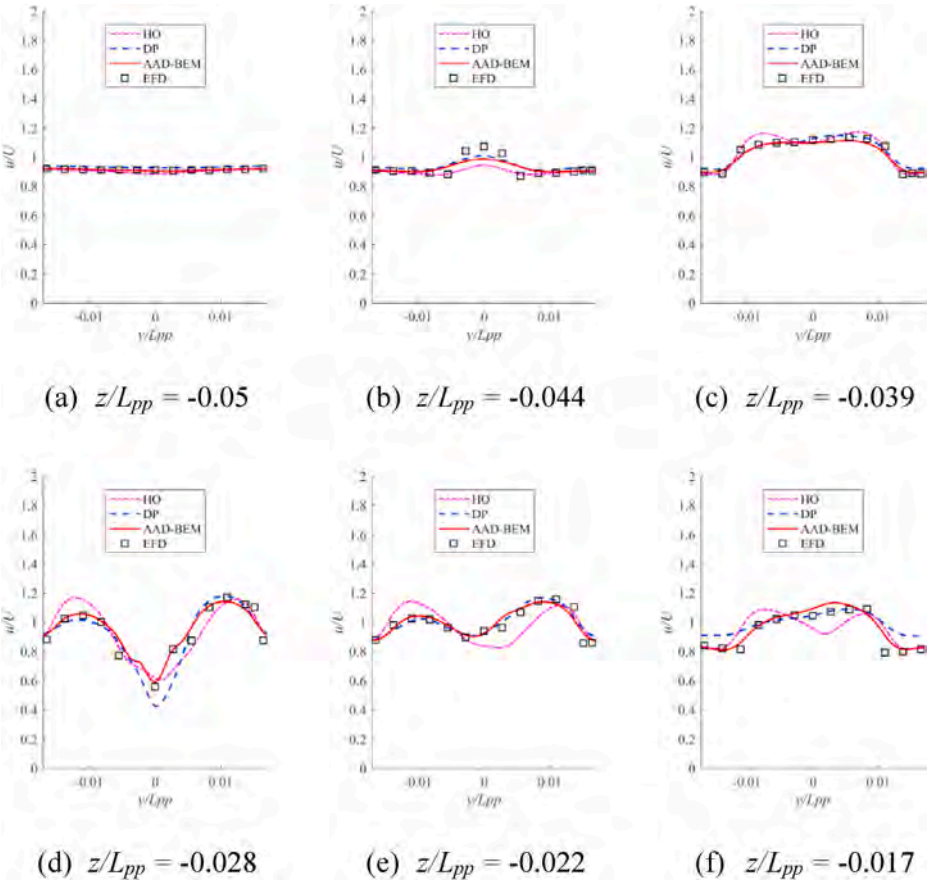

Fig. 35. Comparison of ship wake distributions in different slices.

numerical calculation.

For the convergence analysis of grid size and time-step, according to the advice of International Towing Tank Conference (ITTC), three simulations with different parameter configurations are required. The three simulations correspond to fine, coarse, and medium parameters respectively. S_i is used to represent their calculation results, then the convergence ratio can be expressed as:

$$R = \frac{\varepsilon_{11}}{\varepsilon_{32}} = \frac{S_2 - S_1}{S_3 - S_2} \tag{32}$$

Different R_G correspond to different convergence forms:

Monotonic: $0 < R < 1$;

Oscillatory: $R < 0$;

Divergence: $R > 1$;

For monotonic convergence conditions, the uncertainty can be calculated based on the Richardson Extrapolation (RE). First, the error estimate is:

$$\delta_{RE} = \frac{\varepsilon_{21}}{r^{P_{RE}} - 1} \tag{33}$$

where r represents the refinement ratio. P_{RE} is the estimated order of accuracy, as follows:

$$P_{RE} = \frac{\ln(\varepsilon_{32}/\varepsilon_{21})}{\ln(r)} \tag{34}$$

In addition, the correction coefficient is:

$$C = \frac{r^{P_{RE}} - 1}{r^{P_{Gest}} - 1} \tag{35}$$

where P_{Gest} represents the estimate for the limiting order. According to Stern's paper, $P_{Gest} = 2$ (Naz, 2014) is used in the current studies. Finally, the uncertainty conforming to monotone convergence is:

$$U = \begin{cases} [9.61 -)^2 + 1.1|\delta_{RE}|, 0.875 < C < 1.125 \\ [2|1 - C| + 1]|\delta_{RE}|, 0 < C \le 0.875 \text{ or } C \ge 1.125 \end{cases} \tag{36}$$

For oscillatory convergence, the uncertainty is calculated by the following formula:

$$U = \frac{S_3 - S_2}{2} \tag{37}$$

The validation and verification analysis will be performed using the propeller open-water test at $J = 0.7$ and the ship model resistance test at $Fr = 0.26$. The refinement ratio of grid and time-step are $\sqrt{2}$ and 2. The determined parameters will be used to select the time-step and mesh size of the self-propulsion simulation. Because the body-force model is steady-state, the convergence of time-step of the body-force model is not discussed. The experimental results in the validation and verification refer to the experimental report published by Tokyo 2005) (Hino, 2005).

The validation and verification results are shown in Tables 4–8, which includes results of Experimental Fluid Dynamics (EFD). In the mesh convergence study of the body-force model, the thrust coefficient and the open-water efficiency show oscillation convergence, while the other open-water test results show monotone convergence. Compared with the experimental results, the uncertainty of all the calculated results is less than 2.7%, and the error of the calculation example corresponding to the medium configuration parameters is less than 1.3%. The convergence speed of the body-force model is faster and smoother than that of the discretized propeller. The following propeller mesh is based on the medium grid size configuration. The mesh convergence of the body-force model shows that the current velocity sampling method does not depend on the mesh size.

At the same time, the errors of the total resistance coefficient and the

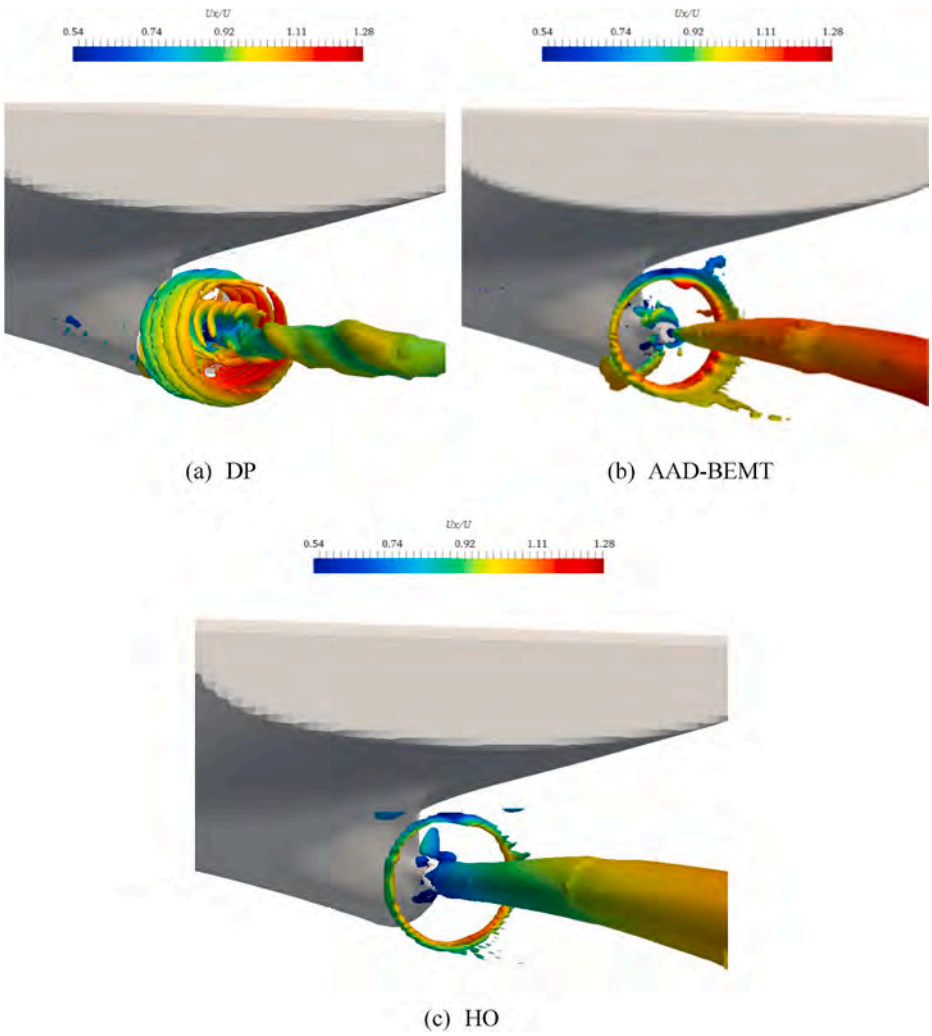

Fig. 36. Comparison of vorticity structures produced by different propeller models.

Table 11
Computational resource of different tests.

Test conditions	Propeller model	Processors	Iteration step	Calculation time (wall clock time)
Propeller open-water test	AAD-BEMT	20	1000	1.72h
	DP	20	2000	19h
Ship self-propulsion test	AAD-BEMT	40	3000	14.2h
	DP	40	6000	147h

wake fraction of the KCS ship are within 2.2% and 2.7% under medium grid conditions, and the grid convergence of pressure resistance and total resistance is oscillatory convergence, while that of friction resistance and wake fraction is monotone convergence. The chosen time-steps in this work have little influence on the resistance calculation of the KCS ship. The errors of total resistance and wake fraction under medium time-step are 1.67% and 2.48%. The friction resistance is monotonic convergence, and the other resistance parameters are oscillation convergence.

Considering the accuracy of calculation and resource consumption, the middle mesh size and time-step have been chosen to carry out the simulation. For the self-propulsion test, the grid distribution of hull and background field is the same as that in the ship resistance test, while the propeller grid and time-step are set according to the discretized propeller open-water test.

4.2. Propeller open-water test

The propeller speed is set to 9.5 r/s in the open-water test, which is the same as the ship model self-propulsion test. To verify the application of the piecewise linear interpolation method in the expression of blade element force coefficient, two series of discretized propeller cases are set up. Series 1 is 0.4–1.0 with seven cases, and series 2 is 0.45–0.95 with six cases. Fig. 19 shows the results of blade element force coefficient under two sets of working conditions. The prediction errors of series 2 by linear piecewise interpolation are all within 4.0% as reported in Table 9. Due to the small second derivative of the force coefficient curve before stall, most interpolation methods are suitable for airfoil data.

In the subsequent sections, the results of the series 1 discretized propeller open-water test are used for providing the data for the AAD-BEMT body-force model. Seven cases of AAD open-water simulation corresponding to Series 1 are conducted for velocity sampling. The velocity distribution of the propeller plane is shown in Fig. 20, and it can be found that the local velocity of the discretized propeller is higher than that of AAD in a large area.

Fig. 21 shows the comparison of local velocity distribution at the propeller plane between the AAD and the discretized propeller. The data of AAD is the velocity at the actuating point in the flow field, while the data of discretized propeller is calculated using the average velocity in the circumferential annular region corresponding to the blade element. It can be found that the distribution of the local velocity is quite different, indicating that the mean value of the flow field of the

discretized propeller cannot be used directly to model source items.

Fig. 22 shows the relationship between velocity parameters and advance ratios in ten different radial positions. The data was calculated and sampled by AAD. Since they are monotone functions, the corresponding relationship can be calculated by piecewise linear interpolation.

Finally, the open-water tests based on AAD-BEMT body-force model is carried out using the blade element velocity relationship and force coefficient information obtained. In this simulation, the body-force model needs to iterate from the initial condition which velocity is the incoming flow to the induced velocity field under the action of propeller. Fig. 23 shows the comparison between numerical and experimental results of open-water curves. It can be found that the trend of propeller open-water performance data predicted by each model is consistent. Since the total load of the descriptive body-force model is the experimental value itself, it is not listed separately. In order to quantify the calculation accuracy of the discretized propeller, Fig. 24 shows the open-water error of the discretized propeller model relative to the experiment. The thrust error is within 1.5%, while the torque error is within 2.0%, which proves the reliability of CFD results of discretized propellers. Since the body-force model is used to replace the discretized propeller model, the open-water error of the body-force model relative to the discretized propeller is investigated, as shown in Fig. 25. The data in Yu et al. (2021) were used for comparison. It can be found that due to the use of the piecewise linear interpolation fitting method and the improvement of the calculation method of the Angle of Attack, the error of AAD-BEMT model is controlled at low and high advance ratios, and the errors at each advance ratio are all within 1%.

Fig. 26 shows the iterative process of the thrust and the torque of the body-force model at each advance ratio, and the black dotted line represents the result of the discretized propeller. Fig. 27 shows the comparison between the load distribution of the body-force model and the discretized propeller model, which shows a high agreement. It is shown that the body-force model can iterate from the initial conditions to the expected steady-state of the flow field, and it is proved that the velocity parameters used to calculate the Angle of Attack by the AAD-BEMT model meet the four conditions proposed above.

To demonstrate the effect of the AAD-BEMT body-force model on the simulation of propeller momentum transport, three sampling lines parallel to the propeller plane are set downstream. The length is the diameter of the propeller. Each sampling line intersected with the propeller shaft and one hundred sampling points are evenly distributed on it. The velocity information at the sampling point is recorded. For the discretized propeller model, as the flow field is unsteady, the data of each sampling point is the average value of 50 moments within one rotation of the propeller. Fig. 28 shows the velocity distribution of the flow field obtained from the sampling line under the action of the body-force model and the discretized propeller. It can be found that the axial velocity distribution of the wake of the discretized propeller is consistent with that of the body-force model, which proves that the body-force model can simulate the downstream momentum transport.

4.3. Ship resistance test

The purpose of ship resistance test simulation is to confirm the accuracy of the discretized hull and to save time by provide an initial condition close to the convergence state of self-propulsion. The simulated condition is set to Fr = 0.26 which is the same as the experiment. To obtain the initial conditions of the self-propulsion, the freedom of heave and pitch is not considered in the resistance test. The accuracy of total resistance and wake fraction has been discussed in the convergence of calculation parameters. Fig. 29 shows the velocity field at the propeller plane. It can be found that the non-uniformity of wake on propeller plane is caused by the shear effect and block effect of the hull surface. The experimental values of the data are also given here. It can be found that the two groups of data are in good agreement.

Fig. 30 and Fig. 31 show the ship wave pattern at Fr = 0.26 of three longitudinal sections in the flow field and ship surface. CFD and EFD represent the results of simulation and experiment respectively. It can be found that the simulation results of the free surface near the hull are consistent with the experimental results.

4.4. Ship self-propulsion test

The working condition of self-propulsion test is Fr = 0.26, without considering the heave and pitch motions. The propeller models used in the self-propulsion test include discretized propeller model, HO model, and AAD-BEMT body-force model. In order to deal with the scale effects of real ship Friction and ship model Friction, Skin Friction Correction (SFC) needs to be set. In the experiment, SFC was set as 30.25N (Hino, 2005). In the self-propulsion test, it is necessary to adjust the propeller rotation speed to achieve a balance between propeller thrust and hull resistance. This paper completes the determination of propeller rotation speed based on the interpolation method proposed by ITTC (2014). The force imbalance is defined as:

$$F_{imblance} = T + SFC - R_T \tag{38}$$

where $F_{imblance}$ is the force imbalance, T is the propeller thrust and R_T is the total ship resistance.

Through the data of force imbalance at different rotation speeds, the target rotation speed when the force unbalance is near zero can be obtained by interpolation method. The force imbalance of different propeller models at different rotation speeds is shown in Fig. 32. Finally, at the selected rotation speed, the force imbalance is less than 1% of the resistance (0.02% for discretized model, 0.05% for the AAD-BEMT model and 0.16% for the HO model), which meets the requirements of ITTC (2014).

Fig. 33 shows the convergence process of propeller thrust under the action of the discretized propeller and the body-force model. The abscissa is the dimensionless iterative step:

$$i^{'} = \frac{i}{I_{total}} \tag{39}$$

where $i^{'}$ is the dimensionless iterative step, I_{total} is the total iteration steps of simulation and i is the iterative step.

Since the HO model adopts the one-time input of propeller load, the thrust force does not change with the flow field iteration. It can be seen that the convergence speed of the AAD-BEMT body-force model is faster than that of the discretized propeller. At the same time, the propeller inflow is no longer circumferential because of the disturbance from the hull, which makes the load fluctuation appear when the propeller blade passes through a specific position. The body-force model based on the time-homogeneity assumption is more stable after the thrust converges. There is a large gap between the HO model thrust and the discretized propeller, because the HO model cannot accurately simulate the thrust reduction caused to the hull, so the thrust is low when the force is balanced.

The calculation results of self-propulsion factors of different propeller models are shown in Table 10. The calculation results of self-propulsion factors show that the simulation results of discretized propellers are the best, in which the errors of resistance coefficient and thrust coefficient are −1.13% and −0.71% respectively. The errors of the AAD-BEMT body-force model are −1.99% and −1.70%. The error of the HO model is the largest, and the error of the resistance and the thrust are −7.98% and −7.22% respectively. The result of the error is expected because the discretized propeller considers the most flow details. At the same time, the HO model ignores the circumferential asymmetry of propeller load, while the AAD-BEMT model considers the influence of un-uniform inflow on propeller load distribution, which has higher accuracy in calculating the self-propulsion factor.

Fig. 34 is the downstream flow field of the propeller. The discretized

propeller is in good agreement with the AAD-BEMT body-force model, while the HO model fails to fully simulate the asymmetry of wake flow. This is due to the hull's blocking effect on tangential flow, which will lead to the redistribution of propeller load, and the descriptive body-force model cannot respond to this effect. The wake distribution characteristics of the AAD-BEMT body-force model are consistent with those of discretized propeller. For quantitative comparison, Fig. 34 shows the axial velocity distribution of wake at different heights. The results of quantitative comparison support the above viewpoint, that is, by properly processing the data accuracy of the AOA and force coefficient, the AAD-BEMT model can reflect the fluid momentum transport around the discretized propeller model while reducing the computational cost (see Fig. 35).

Vorticity structures under different propeller models are reported in Fig. 36, where the definition of vorticity uses the third generation of vortex identification methods: Liutex criterion (Liu et al., 2019). The vortex iso-surface corresponding to $\widetilde{\Omega}_R = 0.52$. The reason for the emergence of tip vortex is that the pressure gradient before and after the propeller makes the fluid near the tip flow back from pressure-side to suction-side, so the intensity of the tip vortex is related to the pressure gradient. For the DP model, the pressure gradient occurs on the surface of blades, and there is no obvious pressure gradient in the gap between the blades. Therefore, the tip vortex are concentrated in the tip and migrate downward with the wake, forming five independent spiral structures. However, for the body-force model, the pressure gradient occurs in the whole propeller plane, so the tip vortex appears a continuous ring structure. At the same time, the pressure force per unit area is smaller for the body-force model, so the tip vortex intensity is weaker than that of the DP model. In addition, the unclosed spiral vortex system is also easier to maintain its own structure during the migration than the closed ring vortex system. The above reasons lead to the rapid dissipation of the body-force model's tip vortex structure. Because the thrust estimated by the HO model is small, the intensity of the tip vortex is smaller and the dissipation is more quickly than that of the AAD-BEMT model. At the same time, because the AAD-BEMT model simulates the asymmetric phenomenon of the wake, the axial length of the vortex structure on the starboard side is longer than that on the port side, which is not significantly different on both sides of the HO model. The above analysis also illustrates that the flow field under the action of the discretized propeller has richer evolution details, so more computing resources are consumed to ensure the accuracy of the simulation.

4.5. Computational cost

The examples in this paper are all carried out with self-developed body force models and discretized propeller model in OpenFOAM, and the relevant work is carried out on the High Performance Computing (HPC) cluster center in Computational Marine Hydrodynamics Lab (CMHL). Each node has 2 CPUs with 20 cores and 64 GB accessible memory (Intel Xeon E5-2680v2 @2.8 GHz). Among them, 20 processes are used in each propeller open-water test. For a single working condition, the iteration step of the AAD-BEMT body-force model is 1000, and the calculation time is 1.72h of wall clock time. The iterative steps of the discretized propeller model are 2000, and the calculation time is 19h of wall clock time. 40 processes are used in ship resistance test and ship self-propulsion test. The iterative step of the self-propulsion test of discretized propeller model is 6000, and the calculation time is 147 h of wall clock time per working condition, while the case of the AAD-BEMT body-force model is 3000, and the calculation time is 14.2h of wall clock time, as shown in Table 11. The above data shows that the AAD-BEMT body-force model has its application value in saving computing resources and at the same time ensuring accuracy.

5. Conclusions

In this paper, a method to obtain the Angle of Attack (AOA) of marine propeller blade element based on Agent Actuating Disk (AAD) is proposed and applied to the application of the Blade Element Momentum Theory (BEMT) body-force model in both propeller open-water test and ship self-propulsion test simulation. For the propeller open-water test simulation, the results show that the discretized propeller model is consistent with the experimental data. The comparison between the results of the AAD-BEMT body-force model and those of the discretized propeller model shows that the thrust, torque, load distribution, and wake evolution of the AAD-BEMT body-force model are in good agreement with the discretized propeller model, which means that the three-dimensional hydrodynamic information of the discretized propeller is accurately reflected in the blade element model of AAD-BEMT method.

For the ship self-propulsion test simulation, AAD-BEMT body-force model, HO body-force model, and discretized propeller model are carried out respectively. The results show that the HO model cannot accurately simulate the characteristics of wake evolution since it does not consider the redistribution of the propeller load in ship-behind conditions. The prediction results of the AAD-BEMT model are in good agreement with that of the discretized propeller model, indicating that the proposed body-force model can simulate the momentum transport of the discretized propeller under un-uniform inflow conditions. The self-propulsion factors are all well predicted with errors within 2%, illustrating that the thrust reduction caused by the AAD-BEMT body-force model and the uneven inflow effect caused by the hull to the propeller are in good agreement with the discretized propeller.

The present work shows that by properly dealing with blade element force coefficient and the accuracy of the AOA of BEMT, the blade element can keep the accuracy of discretized propeller model in a wide range of advance ratios. At the same time, through this kind of data processing, the dish-shaped and mutually independent blade element actuating points can replace the discretized propeller to carry out ship self-propulsion test simulation. However, it is important to realize that the AAD-BEMT model cannot simulate the pulsation effect of the blade continuously sweeping across the stern, which results in the disability of simulating the interaction between the periodic flow structures generated by DP model with other small-scale components. At the same time, the AAD-BEMT model is only for the blade, and the rotation of the hub is not considered. The above problems will affect the accuracy of the flow field simulation around the propeller, so the applicability of the AAD-BEMT model with complex appendages, such as hull-propeller-rudder system, remains to be proved. Future work will focus on the performance of the improved BEMT method in predicting ship maneuverability problems with complex hull-propeller-rudder interactions.

CRediT authorship contribution statement

Mingzhe Wang: Methodology, Investigation, Software, Validation, Data curation, Visualization, Writing – original draft. **Decheng Wan:** Writing – review & editing, Resources, Supervision. **Jianhua Wang:** Conceptualization, Methodology, Investigation, Writing – review & editing, Supervision.

Declaration of competing interest

The authors declare that they have no known competing financial interests or personal relationships that could have appeared to influence the work reported in this paper.

Data availability

Data will be made available on request.

Acknowledgements

This work was supported by the National Key Research and Development Program of China(2019YFB1704200), and the National Natural Science Foundation of China (51809169), to which the authors are most grateful.

References

Benini, E., 2004. Significance of blade element theory in performance prediction of marine propellers. Ocean Eng. 31 (8–9), 957–974. https://doi.org/10.1016/j.oceaneng.2003.12.001.

Broglia, R., Dubbioso, G., Durante, D., Mascio, A.D., 2013. Simulation of turning circle by CFD: analysis of different propeller models and their effect on manoeuvring prediction. Appl. Ocean Res. 39, 1–10. https://doi.org/10.1016/j.apor.2012.09.001.

Berberović, E., van Hinsberg, N., Jakirlić, S., Roisman, I., Tropea, C., 2009. Drop impact onto a liquid layer of finite thickness dynamics of the cavity evolution. Phys. Rev. E 79 (3), 36306.

Churchfield, M., Lee, S., 2013. NWTC Design Codes (SOWFA). http://wind.nrel.gov/designcodes/simulators/SOWFA.

Feng, D., Yu, J., He, R., Zhang, Z., Wang, X., 2020a. Free running computations of KCS with different propulsion models. Ocean Eng. 214 https://doi.org/10.1016/j.oceaneng.2020.107563.

Feng, D., Yu, J., He, R., Zhang, Z., Wang, X., 2020b. Improved body force propulsion model for ship propeller simulation. Appl. Ocean Res. 104 https://doi.org/10.1016/j.apor.2020.102328.

Fu, H., Michael, T.J., Carrica, P.M., 2015. A method to perform self-propulsion computations with a simplified body-force propeller model. In: Proceedings of the Twenty-Fifth International Ocean and Polar Engineering Conference. Kona, Big Island, Hawaii, USA.

Guo, C., Wang, X., Wang, C., Zhao, Q., Zhang, H., 2020. Research on calculation methods of ship model self-propulsion prediction. Ocean Eng. 203, 107232 https://doi.org/10.1016/j.oceaneng.2020.107232.

Hino, T. (Ed.), 2005. Proceedings of CFD Workshop Tokyo 2005. National Maritime Research Institute.

Hough, G., Ordway, D., 1965. The generalized actuator disk. Dev. Theor. Appl. Mech. 2, 317–336.

ITTC, 2014. Practical guidelines for ship self-propulsion CFD. Recommended Procedures and Guidelines. No. 7.5-03-03-01.

Kim, I.-T., Kim, C., Kim, S.-H., Ko, D., Moon, S.-H., Park, H., Jin, B., 2021. Estimation of the maneuverability of the KVLCC2 in calm water using free running simulation based on CFD. Int. J. Nav. Archit. Ocean Eng. 13, 466–477. https://doi.org/10.1016/j.ijnaoe.2021.05.004.

Li, Z., Yu, J., Feng, D., Jiang, K., Zhou, Y., 2019. Research on the improved body-force method based on viscous flow. In: Proceedings of the ASME 2019 38th International Conference on Ocean, Offshore and Arctic Engineering. Glasgow, Scotland, UK.

Liu, C., Gao, Y.-s., Dong, X.-r., Wang, Y.-q., Liu, J.-m., Zhang, Y.-n., Gui, N., 2019. Third generation of vortex identification methods: omega and Liutex/Rortex based systems. J. Hydrodyn. 31 (2), 205–223. https://doi.org/10.1007/s42241-019-0022-4.

Liu, X.-w., Chen, S.-t., Zhao, W.-w., Wan, D.-c., Wang, Y.-q., 2021. Liutex-based centripetal force field model for improving the resistance and wake performances of JBC ship sailing in calm water. J. Hydrodyn. 33 (3), 494–502. https://doi.org/10.1007/s42241-021-0046-4.

Melani, P.F., Balduzzi, F., Ferrara, G., Bianchini, A., 2020. How to extract the angle attack on airfoils in cycloidal motion from a flow field solved with computational fluid dynamics? Development and verification of a robust computational procedure. Energy Convers. Manag. 223, 113284 https://doi.org/10.1016/j.enconman.2020.113284.

Menter, F.R., 1994. Two-equation eddy-viscosity turbulence models for engineering applications. AIAA J. 32 (8), 1598–1605.

Moukalled, F., Mangani, L., Darwish, M., 2016. The Finite Volume Method in Computational Fluid Dynamics: an Advanced Introduction with OpenFOAM® and Matlab, 113. Springer International Publishing. https://doi.org/10.1007/978-3-319-16874-6.

Naing Win, Y., Wu, P.-C., Akamatsu, K., Okawa, H., Stern, F., Toda, Y., 2016. RANS simulation of KVLCC2 using simple body-force propeller model with rudder and without rudder. J. Jpn. Soc. Nav. Archit. Ocean Eng. 23, 1–11. https://doi.org/10.2534/jjasnaoe.23.1.

Naz, N., 2014. Numerical Simulation of Flow Around Ship Hull Considering Rudder-Propeller Interaction. Bangladesh university of engineering and technology.

Ortolani, F., Dubbioso, G., Muscari, R., Mauro, S., Di Mascio, A., 2018. Experimental and numerical investigation of propeller loads in off-design conditions. J. Mar. Sci. Eng. 6 (2) https://doi.org/10.3390/jmse6020045.

Phillips, A.B., Turnock, S.R., Furlong, M., 2009. Evaluation of manoeuvring coefficients of a self-propelled ship using a blade element momentum propeller model coupled to a Reynolds averaged Navier Stokes flow solver. Ocean Eng. 36 (15–16), 1217–1225. https://doi.org/10.1016/j.oceaneng.2009.07.019.

Phillips, A.B., Turnock, S.R., Furlong, M., 2010. Accurate capture of propeller-rudder interaction using a coupled blade element momentum-RANS approach. Ship Technol. Res. 57 (2), 128–139. https://doi.org/10.1179/str.2010.57.2.005.

Posa, A., Broglia, R., 2019. An immersed boundary method coupled with a dynamic overlapping-grids strategy. Comput. Fluids 191, 104250. https://doi.org/10.1016/j.compfluid.2019.104250.

Ren, Z., Wang, J., Wan, D., Abdel-Maksoud, M., 2020. Numerical investigation of propeller-rudder interaction based on body force approach. In: Proceedings of the Thirtieth (2020) International Ocean and Polar Engineering Conference. Shanghai, China.

Shen, W.Z., Hansen, M.O.L., Sørensen, J.N., 2009. Determination of the angle of attack on rotor blades. Wind Energy 12 (1), 91–98. https://doi.org/10.1002/we.277.

Shen, Z., Wan, D.C., 2013. RANS computations of added resistance and motions of a ship in head waves. Int. J. Offshore Polar Eng. 23, 264–271.

Shen, Z., Ye, H., Wan, D.C., 2014. URANS simulations of ship motion responses in long-crest irregular waves. J. Hydrodynam. Ser. B 26, 436–446. https://doi.org/10.1016/S1001-6058(14)60050-0.

Shen, Z., Wan, D., Carrica, P.M., 2015. Dynamic overset grids in OpenFOAM with application to KCS self-propulsion and maneuvering. Ocean Eng. 108, 287–306. https://doi.org/10.1016/j.oceaneng.2015.07.035.

Shen, Z., Wan, D.C., 2016. An irregular wave generating approach based on naoe-FOAM-SJTU solver. China Ocean Eng. 30, 177–192.

Simonsen, C.D., Stern, F., 2005. RANS maneuvering simulation of Esso Osaka with rudder and a body-force propeller. J. Ship Res. 49 (2), 98–120. https://doi.org/10.5957/jsr.2005.49.2.98.

Stern, F., Wilson, R.V., Coleman, H.W., Paterson, E.G., 2001. Comprehensive approach to verification and validation of CFD simulations—Part 1: methodology and procedures. J. Fluid Eng. 123 (4), 793–802. https://doi.org/10.1115/1.1412235.

Tokgoz, E., Win, Y.N., Kuroda, K., Toda, Y., 2014. A new method to predict the propeller body-force distribution for modeling the propeller in viscous CFD code without potential flow code. J. Jpn. Soc. Nav. Archit. Ocean Eng. 19, 1–7.

Tu, T.N., 2019. Numerical simulation of propeller open-water characteristics using RANSE method. Alex. Eng. J. 58 (2), 531–537. https://doi.org/10.1016/j.aej.2019.05.005.

Villa, D., Franceschi, A., Viviani, M., 2020. Numerical analysis of the rudder–propeller interaction. J. Mar. Sci. Eng. 8 (12) https://doi.org/10.3390/jmse8120990.

Villa, D., Viviani, M., Tani, G., Gaggero, S., Bruzzone, D., Podenzana, C.B., 2018. Numerical evaluation of rudder performance behind a propeller in bollard pull condition. J. Mar. Sci. Appl. 17 (2), 153–164. https://doi.org/10.1007/s11804-018-0018-4.

Vimalakanthan, K., Schepers, J.G., Shen, W.Z., Rahimi, H., Micallef, D., Simao Ferreira, C.J., Klein, L., 2018. Evaluation of different methods of determining the Angle of Attack on wind turbine blades under yawed inflow conditions. J. Phys. Conf. 1037 https://doi.org/10.1088/1742-6596/1037/2/022028.

Wang, J., Wan, D., 2018. CFD investigations of ship maneuvering in waves using naoe-FOAM-SJTU solver. J. Mar. Sci. Appl. 17 (3), 443–458. https://doi.org/10.1007/s11804-018-0042-4.

Wang, J., Zhao, W., Wan, D., 2019. Development of naoe-FOAM-SJTU solver based on OpenFOAM for marine hydrodynamics. J. Hydrodyn. 31 (1), 1–20. https://doi.org/10.1007/s42241-019-0020-6.

Wang, J., Wan, D., 2020. CFD study of ship stopping maneuver by overset grid technique. Ocean Eng. 197, 106895 https://doi.org/10.1016/j.oceaneng.2019.106895.

Win, Y.N., Wu, P.C., Toda, Y., Tokgoz, E., Stern, F., 2013. Computation of propeller-hull interaction using simple body-force distribution model around series 60 C_B = 0.6. J. Jpn. Soc. Nav. Archit. Ocean Eng. 18, 17–27.

Windén, B., Kawamura, T., Huang, Z., 2015. Comparative Self Propulsion Simulations of the JBC Bulk Carrier, 20. Conference Proceedings The Japan Society of Naval Architects and Ocean Engineers.

Xing, T., Stern, F., 2010. Factors of safety for Richardson extrapolation. J. Fluid Eng. 132 (6), 061403 https://doi.org/10.1115/1.4001771.

Yamazaki, R., 1977. On the Propulsion Theory of Ships on Still Water (Improved Theoretical Method), 1. Memoirs Of The Kyushu University, Faculty of Engineering, pp. 65–88, 34.

Yao, J., Liu, Z., Song, X., Su, Y., 2021. Ship manoeuvring prediction with hydrodynamic derivatives from RANS: development and application. Ocean Eng. 231, 109036 https://doi.org/10.1016/j.oceaneng.2021.109036.

Yu, H.-d., Wang, Y.-q., 2020. Liutex-based vortex dynamics: a preliminary study. J. Hydrodyn. 32 (6), 1217–1220. https://doi.org/10.1007/s42241-020-0084-3.

Yu, J., Yao, C., Liu, L., Zhang, Z., Feng, D., 2021. Assessment of full-scale KCS free running simulation with body-force models. Ocean Eng. 237, 109570 https://doi.org/10.1016/j.oceaneng.2021.109570.

Zha, R., Ye, H., Shen, Z., Wan, D.C., 2014. Numerical study of viscous wave-making resistance of ship navigation in still water. J. Mar. Sci. Appl. 13, 158–166. https://doi.org/10.1007/s11804-014-1248-8.

Zha, R., Ye, H., Shen, Z., Wan, D.C., 2015. Numerical computations of resistance of high speed catamaran in calm water. J. Hydrodynam. Ser. B 26, 930–938. https://doi.org/10.1016/S1001-6058(14)60102-5.

Zhang, Z.-r., 2010. Verification and validation for RANS simulation of KCS container ship without/with propeller. J. Hydrodyn. 22 (5), 889–896. https://doi.org/10.1016/s1001-6058(10)60055-8.